Single scattering by a small volume element

Michael I. Mishchenko

NASA Goddard Institute for Space Studies, 2880 Broadway, New York, New York 10025

Joop W. Hovenier

Astronomical Institute "Anton Pannekoek," University of Amsterdam, Kruislaan 403, 1098 SJ Amsterdam, The Netherlands

Daniel W. Mackowski

Department of Mechanical Engineering, 201 Ross Hall, Auburn University, Auburn, Alabama 36849-5341

Received April 20, 2003; revised manuscript received July 29, 2003; accepted August 26, 2003

Starting from first principles, we present a detailed analysis of the concept of single scattering of light by a small volume element filled with sparsely and randomly positioned particles. We first derive the formulas of the far-field single-scattering approximation, which treats the volume element as a single scatterer, and discuss its range of applicability, using for illustration exact T-matrix results for randomly oriented two-sphere clusters. Our second approach is to treat the volume element as a small cloud of particles and apply the so-called first-order-scattering approximation. We demonstrate that although the two approaches are based on somewhat different sets of assumptions, they give essentially the same result for the electromagnetic response of a sufficiently distant polarization-sensitive detector.

OCIS codes: 290.0290, 290.5850, 290.4210, 260.2110, 260.5430, 030.5620.

1. INTRODUCTION

The concept of single scattering of light by a small volume element filled with sparsely and randomly positioned particles has been central to the disciplines of electromagnetic scattering by small particles and phenomenological radiative transfer.[1–18] Yet it appears that while the same terminology is widely used in the scientific literature, the specific meaning of this concept remains rather vague and seems to vary from publication to publication. With the development of the microphysical approach to radiative transfer (see Ref. 19 and references therein), the small (or "differential") volume element has completely lost its long-cherished role as an elementary scattering unit in a macroscopic medium composed of randomly positioned discrete particles. Now the role of the elementary scatterers rightfully belongs to the scattering particles themselves, which, with the benefit of hindsight, one should have expected. However, the concept of a small volume element remains a useful modeling tool in practical applications in which (1) the scattering medium is observed from a distance much greater than its maximal linear dimension and (2) the number of particles is insufficiently large to cause a significant multiple-scattering component of the total scattered radiation. A prime example of such applications is the analysis and interpretation of laboratory measurements of light scattering by tenuous collections of natural and artificial small particles (e.g., Refs. 20–23 and references therein). Therefore the objective of this paper is to present a detailed and consistent analysis of scattering by a small volume element starting from first principles. Specifically, we discuss how one can model theoretically the response of a polarization-sensitive well-collimated detector placed at a large distance from a small volume element filled with randomly and sparsely distributed discrete scatterers.

We begin by deriving and discussing the formulas of the far-field single-scattering approximation, which treats the small volume element as a single, albeit "random" scatterer. We then take an alternative look at the problem by treating the volume element as a small cloud of particles, using the concepts originating in the microphysical approach to radiative transfer,[19] and applying the so-called first-order-scattering approximation. The final section discusses the relation between these two approaches and compares their ranges of applicability.

2. FAR-FIELD SCATTERING BY A SINGLE FIXED PARTICLE

The aim of this section is to make the paper reasonably self-contained by briefly introducing the necessary definitions and notation and listing the equations describing far-field electromagnetic scattering by a single particle. An extensive discussion of the subjects covered, including explicit derivations of all formulas, can be found in Ref. 7 (hereinafter referred to as MTL). We will assume that all fields are time harmonic and will omit the common factor $\exp(-i\omega t)$, where t is time and ω is angular frequency. 3-vectors will be denoted with bold roman letters, whereas matrices will be denoted with bold sans serif letters.

A. Stokes Parameters

To introduce various characteristics of a transverse electromagnetic wave, we use the local right-handed Carte-

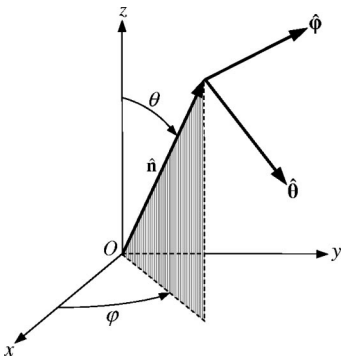

Fig. 1. Local coordinate system used to describe the direction of propagation and the polarization state of a transverse electromagnetic wave at the observation point O.

sian coordinate system with origin at the observation point, as shown in Fig. 1, and specify the direction of propagation of the wave by a unit vector $\hat{\mathbf{n}}$ or, alternatively, by a couple $\{\theta, \varphi\}$, where $\theta \in [0, \pi]$ is the polar angle and $\varphi \in [0, 2\pi)$ is the azimuth angle. The electric field at the observation point can be expressed as $\mathbf{E} = \mathbf{E}_\theta + \mathbf{E}_\varphi = E_\theta \hat{\boldsymbol{\theta}} + E_\varphi \hat{\boldsymbol{\varphi}}$, where $\mathbf{E}_\theta$ and $\mathbf{E}_\varphi$ are the θ and φ components of the electric field vector, respectively, and $\hat{\boldsymbol{\theta}}$ and $\hat{\boldsymbol{\varphi}}$ are the corresponding unit vectors.

Let a plane electromagnetic wave propagate in a homogeneous isotropic medium with a real electric permittivity ε and a real magnetic susceptibility μ:

$$\mathbf{E}(\mathbf{r}) = \mathbf{E}_0 \exp(ik\hat{\mathbf{n}} \cdot \mathbf{r}), \qquad \mathbf{E}_0 \cdot \hat{\mathbf{n}} = 0, \tag{1}$$

where $\hat{\mathbf{n}}$ is a unit vector in the propagation direction and $k = \omega\sqrt{\varepsilon\mu}$ is the (real) wave number. The Stokes parameters I, Q, U, and V of the wave form the 4×1 column Stokes vector $\mathbf{I}$ according to

$$\mathbf{I} = \begin{pmatrix} I \\ Q \\ U \\ V \end{pmatrix} = \frac{1}{2}\left(\frac{\varepsilon}{\mu}\right)^{1/2} \begin{pmatrix} E_{0\theta}E_{0\theta}^* + E_{0\varphi}E_{0\varphi}^* \\ E_{0\theta}E_{0\theta}^* - E_{0\varphi}E_{0\varphi}^* \\ -E_{0\theta}E_{0\varphi}^* - E_{0\varphi}E_{0\theta}^* \\ \mathrm{i}(E_{0\varphi}E_{0\theta}^* - E_{0\theta}E_{0\varphi}^*) \end{pmatrix}, \tag{2}$$

where an asterisk denotes complex conjugation, and have the dimension of monochromatic energy flux. Since traditional optical devices cannot measure the electric field associated with a beam of light, the Stokes parameters provide the most complete characterization of a transverse electromagnetic wave, inasmuch as it is subject to practical analysis.

B. Coherency Dyad

The definition of the Stokes vector explicitly exploits the transverse character of an electromagnetic wave and requires the use of a local spherical coordinate system. However, in some cases it is convenient to introduce an alternative quantity, which also provides a complete optical specification of a transverse electromagnetic wave but is defined without explicit use of a coordinate system. This quantity is called the coherency dyad and is given by

$$\vec{\rho} = \mathbf{E} \otimes \mathbf{E}^* = \mathbf{E}_0 \otimes \mathbf{E}_0^*, \tag{3}$$

where $\otimes$ denotes the dyadic product of two vectors. It is then clear that the Stokes vector can be expressed in terms of the coherency dyad as follows:

$$\mathbf{I} = \frac{1}{2}\left(\frac{\varepsilon}{\mu}\right)^{1/2} \begin{pmatrix} \hat{\boldsymbol{\theta}} \cdot \vec{\rho} \cdot \hat{\boldsymbol{\theta}} + \hat{\boldsymbol{\varphi}} \cdot \vec{\rho} \cdot \hat{\boldsymbol{\varphi}} \\ \hat{\boldsymbol{\theta}} \cdot \vec{\rho} \cdot \hat{\boldsymbol{\theta}} - \hat{\boldsymbol{\varphi}} \cdot \vec{\rho} \cdot \hat{\boldsymbol{\varphi}} \\ -\hat{\boldsymbol{\theta}} \cdot \vec{\rho} \cdot \hat{\boldsymbol{\varphi}} - \hat{\boldsymbol{\varphi}} \cdot \vec{\rho} \cdot \hat{\boldsymbol{\theta}} \\ \mathrm{i}(\hat{\boldsymbol{\varphi}} \cdot \vec{\rho} \cdot \hat{\boldsymbol{\theta}} - \hat{\boldsymbol{\theta}} \cdot \vec{\rho} \cdot \hat{\boldsymbol{\varphi}}) \end{pmatrix}, \tag{4}$$

whereas $\vec{\rho} \cdot \hat{\mathbf{n}}$ and $\hat{\mathbf{n}} \cdot \vec{\rho}$ vanish.

The coherency dyad is a more general quantity than the Stokes vector because it can be applied to any electromagnetic field and not just to a transverse electromagnetic wave. This makes the coherency dyad convenient in studies of electromagnetic fields created by groups of scatterers. However, it is important to remember that when the coherency dyad is applied to an arbitrary electromagnetic field, it may not always have as definite a physical meaning as that of, for example, the Poynting vector. The relationship between the coherency dyad and the actual physical observables may change depending on the problem at hand and must be carefully established whenever this quantity is used in a theoretical analysis of a specific measurement procedure.[19]

C. Far-Field Scattering by a Single Particle

Consider a scattering particle embedded in an infinite, homogeneous, linear, isotropic, and nonabsorbing medium (Fig. 2). The scatterer occupies a finite interior region V_{INT} and is surrounded by the infinite exterior region. The interior region is filled with an isotropic, linear, and possibly inhomogeneous material. Assuming that the host medium and the scatterer are nonmagnetic [i.e., $\mu_2(\mathbf{r}) = \mu_1 = \mu_0$, where the subscripts 1 and 2 correspond to the host medium and the scatterer, respectively, and μ_0 is the permeability of a vacuum], one can show that the total electric field everywhere in space satisfies the following volume integral equation:

$$\mathbf{E}(\mathbf{r}) = \mathbf{E}^{\mathrm{inc}}(\mathbf{r}) + k_1^2 \int_{V_{\mathrm{INT}}} \mathrm{d}\mathbf{r}'\, \vec{G}(\mathbf{r}, \mathbf{r}') \cdot \mathbf{E}(\mathbf{r}')[m^2(\mathbf{r}') - 1], \qquad \mathbf{r} \in \Re^3, \tag{5}$$

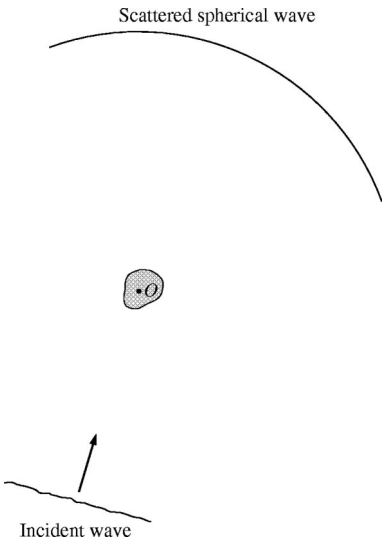

Fig. 2. Schematic representation of the electromagnetic scattering problem. The unshaded exterior region is unbounded in all directions, whereas the shaded area represents the interior region V_{INT}.

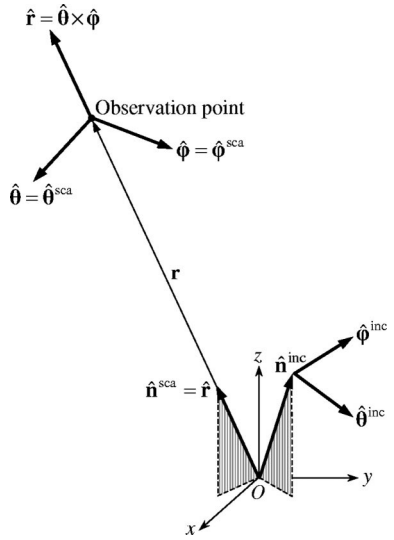

Fig. 3. Far-field scattering by a single particle.

where $\mathbf{E}^{\mathrm{inc}}(\mathbf{r})$ is the incident field,

$$\vec{G}(\mathbf{r}, \mathbf{r}') = \left(\vec{I} + \frac{1}{k_1^2} \nabla \otimes \nabla \right) \frac{\exp(ik_1|\mathbf{r} - \mathbf{r}'|)}{4\pi|\mathbf{r} - \mathbf{r}'|} \tag{6}$$

is the free-space dyadic Green's function, $\vec{I}$ is the identity dyad, and $m(\mathbf{r}) = k_2(\mathbf{r})/k_1$ is the refractive index of the interior relative to that of the exterior. Alternatively, the scattered field $\mathbf{E}^{\mathrm{sca}}(\mathbf{r}) = \mathbf{E}(\mathbf{r}) - \mathbf{E}^{\mathrm{inc}}(\mathbf{r})$ can be expressed in terms of the incident field by means of the so-called dyad transition operator $\vec{T}$:

$$\mathbf{E}^{\mathrm{sca}}(\mathbf{r}) = \int_{V_{\mathrm{INT}}} d\mathbf{r}' \, \vec{G}(\mathbf{r}, \mathbf{r}') \cdot \int_{V_{\mathrm{INT}}} d\mathbf{r}'' \, \vec{T}(\mathbf{r}', \mathbf{r}'') \cdot \mathbf{E}^{\mathrm{inc}}(\mathbf{r}''), \qquad \mathbf{r} \in \Re^3. \tag{7}$$

Substituting Eq. (7) into Eq. (5) yields the Lippmann–Schwinger equation for $\vec{T}$:

$$\vec{T}(\mathbf{r}, \mathbf{r}') = k_1^2[m^2(\mathbf{r}) - 1]\delta(\mathbf{r} - \mathbf{r}')\vec{I} + k_1^2[m^2(\mathbf{r}) - 1] \int_{V_{\mathrm{INT}}} d\mathbf{r}'' \, \vec{G}(\mathbf{r}, \mathbf{r}'') \cdot \vec{T}(\mathbf{r}'', \mathbf{r}'), \qquad \mathbf{r}, \mathbf{r}' \in V_{\mathrm{INT}}, \tag{8}$$

where $\delta(\mathbf{r})$ is the three-dimensional Dirac delta function.

Let us now choose a point O close to the geometrical center of the scattering particle as the common origin of all position vectors (Figs. 2 and 3) and make the following far-field assumptions:

$$r \gg a, \tag{9}$$

$$r \gg k_1 a^2/2, \tag{10}$$

$$k_1 r \gg 1, \tag{11}$$

where $r = |\mathbf{r}|$ and a is the radius of the smallest circumscribing sphere of the scatterer. Then Eq. (5) becomes

$$\mathbf{E}^{\mathrm{sca}}(\mathbf{r}) = \frac{\exp(ik_1 r)}{r} \frac{k_1^2}{4\pi} (\vec{I} - \hat{\mathbf{r}} \otimes \hat{\mathbf{r}}) \cdot \int_{V_{\mathrm{INT}}} d\mathbf{r}' \times [m^2(\mathbf{r}') - 1]\mathbf{E}(\mathbf{r}')\exp(-ik_1 \hat{\mathbf{r}} \cdot \mathbf{r}'). \tag{12}$$

The factor $\vec{I} - \hat{\mathbf{r}} \otimes \hat{\mathbf{r}}$ ensures that the scattered spherical wave in the far-field zone is transverse, so that

$$\mathbf{E}^{\mathrm{sca}}(\mathbf{r}) = \frac{\exp(ik_1 r)}{r} \mathbf{E}_1^{\mathrm{sca}}(\hat{\mathbf{r}}), \qquad \hat{\mathbf{r}} \cdot \mathbf{E}_1^{\mathrm{sca}}(\hat{\mathbf{r}}) = 0, \tag{13}$$

where the scattering amplitude $\mathbf{E}_1^{\mathrm{sca}}(\hat{\mathbf{r}})$ is independent of r and describes the angular distribution of the scattered radiation.

Note that the inequality (9) requires the observation point to be located at a distance from the particle much greater than the particle size. Therefore, when the partial wavelets generated by infinitesimally small volume elements constituting the particle arrive at the observation point, they propagate in essentially the same scattering direction. The inequality (10) can be interpreted as the requirement that the observation point be so far from the scatterer that the phase difference between the paths connecting the observation point and any two points of the scatterer becomes independent of r for any fixed scattering direction. As a result, the surfaces of constant phase of the partial wavelets coincide in the far-field zone, and the partial wavelets form a single outgoing spherical wave. Finally, the inequality (11) means that the distance to the observation point must be much greater than the wavelength.

Assuming that the incident field is a plane wave, that is,

$$\mathbf{E}^{\mathrm{inc}}(\mathbf{r}) = \mathbf{E}_0^{\mathrm{inc}} \exp(ik_1 \hat{\mathbf{n}}^{\mathrm{inc}} \cdot \mathbf{r}), \tag{14}$$

we have

$$\mathbf{E}_1^{\mathrm{sca}}(\hat{\mathbf{n}}^{\mathrm{sca}}) = \vec{A}(\hat{\mathbf{n}}^{\mathrm{sca}}, \hat{\mathbf{n}}^{\mathrm{inc}}) \cdot \mathbf{E}_0^{\mathrm{inc}}, \tag{15}$$

where $\hat{\mathbf{n}}^{\mathrm{sca}} = \hat{\mathbf{r}}$ (Fig. 3). The elements of the scattering dyad $\vec{A}(\hat{\mathbf{n}}^{\mathrm{sca}}, \hat{\mathbf{n}}^{\mathrm{inc}})$ have the dimension of length. It follows from Eq. (13) that

$$\hat{\mathbf{n}}^{\mathrm{sca}} \cdot \vec{A}(\hat{\mathbf{n}}^{\mathrm{sca}}, \hat{\mathbf{n}}^{\mathrm{inc}}) = 0. \tag{16}$$

Since $\mathbf{E}_0^{\mathrm{inc}} \cdot \hat{\mathbf{n}}^{\mathrm{inc}} = 0$, the dot product $\vec{A}(\hat{\mathbf{n}}^{\mathrm{sca}}, \hat{\mathbf{n}}^{\mathrm{inc}}) \cdot \hat{\mathbf{n}}^{\mathrm{inc}}$ is not defined by Eq. (15). To complete the definition, we take this product to be zero:

$$\vec{A}(\hat{\mathbf{n}}^{\mathrm{sca}}, \hat{\mathbf{n}}^{\mathrm{inc}}) \cdot \hat{\mathbf{n}}^{\mathrm{inc}} = 0. \tag{17}$$

Equations (16) and (17) allow one to introduce the 2×2 amplitude matrix $\mathbf{S}$, which describes the transformation of the θ and φ components of the incident plane wave into the θ and φ components of the scattered spherical wave (Fig. 3):

$$\mathbf{E}^{\mathrm{sca}}(r\hat{\mathbf{n}}^{\mathrm{sca}}) = \frac{\exp(ik_1 r)}{r} \mathbf{S}(\hat{\mathbf{n}}^{\mathrm{sca}}, \hat{\mathbf{n}}^{\mathrm{inc}}) \mathbf{E}_0^{\mathrm{inc}}, \tag{18}$$

where $\mathbf{E}$ denotes a two-component column formed by the θ and φ components of the electric vector, i.e.,

$$\mathbf{E} = \begin{pmatrix} E_\theta \\ E_\varphi \end{pmatrix}. \tag{19}$$

The elements of the amplitude matrix have the dimension of length and are expressed in terms of the scattering dyad as follows:

$$S_{11} = \hat{\boldsymbol{\theta}}^{\rm sca} \cdot \vec{A} \cdot \hat{\boldsymbol{\theta}}^{\rm inc}, \qquad S_{12} = \hat{\boldsymbol{\theta}}^{\rm sca} \cdot \vec{A} \cdot \hat{\boldsymbol{\varphi}}^{\rm inc},$$

$$S_{21} = \hat{\boldsymbol{\varphi}}^{\rm sca} \cdot \vec{A} \cdot \hat{\boldsymbol{\theta}}^{\rm inc}, \qquad S_{22} = \hat{\boldsymbol{\varphi}}^{\rm sca} \cdot \vec{A} \cdot \hat{\boldsymbol{\varphi}}^{\rm inc}. \tag{20}$$

D. Phase and Extinction Matrices

Although the amplitude matrix provides a complete specification of the scattering process in the far-field zone, the elements of the amplitude matrix cannot be measured with a typical optical instrument. It is, therefore, useful to characterize the scattering process in terms of actual observables related to the Stokes parameters.

Consider two orientations of a well-collimated Stokes meter in the far-field zone of a particle as shown in Fig. 4. Specifically, detector 1 captures both the incident and the scattered light, whereas detector 2 receives only the scattered light. To describe the response of detector 2, we define the Stokes parameters of the incident plane wave and the scattered spherical wave as

$$\mathbf{I}^{\rm inc} = \begin{pmatrix} I^{\rm inc} \\ Q^{\rm inc} \\ U^{\rm inc} \\ V^{\rm inc} \end{pmatrix} = \frac{1}{2}\left(\frac{\varepsilon_1}{\mu_0}\right)^{1/2} \begin{pmatrix} E_{0\theta}^{\rm inc} E_{0\theta}^{\rm inc*} + E_{0\varphi}^{\rm inc} E_{0\varphi}^{\rm inc*} \\ E_{0\theta}^{\rm inc} E_{0\theta}^{\rm inc*} - E_{0\varphi}^{\rm inc} E_{0\varphi}^{\rm inc*} \\ -E_{0\theta}^{\rm inc} E_{0\varphi}^{\rm inc*} - E_{0\varphi}^{\rm inc} E_{0\theta}^{\rm inc*} \\ \mathrm{i}(E_{0\varphi}^{\rm inc} E_{0\theta}^{\rm inc*} - E_{0\theta}^{\rm inc} E_{0\varphi}^{\rm inc*}) \end{pmatrix}, \tag{21}$$

$$\mathbf{I}^{\rm sca}(r\hat{\mathbf{n}}^{\rm sca}) = \begin{pmatrix} I^{\rm sca}(r\hat{\mathbf{n}}^{\rm sca}) \\ Q^{\rm sca}(r\hat{\mathbf{n}}^{\rm sca}) \\ U^{\rm sca}(r\hat{\mathbf{n}}^{\rm sca}) \\ V^{\rm sca}(r\hat{\mathbf{n}}^{\rm sca}) \end{pmatrix} = \frac{1}{r^2}\frac{1}{2}\left(\frac{\varepsilon_1}{\mu_0}\right)^{1/2} \begin{pmatrix} E_{1\theta}^{\rm sca}(\hat{\mathbf{n}}^{\rm sca})[E_{1\theta}^{\rm sca}(\hat{\mathbf{n}}^{\rm sca})]^* + E_{1\varphi}^{\rm sca}(\hat{\mathbf{n}}^{\rm sca})[E_{1\varphi}^{\rm sca}(\hat{\mathbf{n}}^{\rm sca})]^* \\ E_{1\theta}^{\rm sca}(\hat{\mathbf{n}}^{\rm sca})[E_{1\theta}^{\rm sca}(\hat{\mathbf{n}}^{\rm sca})]^* - E_{1\varphi}^{\rm sca}(\hat{\mathbf{n}}^{\rm sca})[E_{1\varphi}^{\rm sca}(\hat{\mathbf{n}}^{\rm sca})]^* \\ -E_{1\theta}^{\rm sca}(\hat{\mathbf{n}}^{\rm sca})[E_{1\varphi}^{\rm sca}(\hat{\mathbf{n}}^{\rm sca})]^* - E_{1\varphi}^{\rm sca}(\hat{\mathbf{n}}^{\rm sca})[E_{1\theta}^{\rm sca}(\hat{\mathbf{n}}^{\rm sca})]^* \\ \mathrm{i}\{E_{1\varphi}^{\rm sca}(\hat{\mathbf{n}}^{\rm sca})[E_{1\theta}^{\rm sca}(\hat{\mathbf{n}}^{\rm sca})]^* - E_{1\theta}^{\rm sca}(\hat{\mathbf{n}}^{\rm sca})[E_{1\varphi}^{\rm sca}(\hat{\mathbf{n}}^{\rm sca})]^*\} \end{pmatrix}, \tag{22}$$

respectively, where $\hat{\mathbf{n}}^{\rm sca} \neq \hat{\mathbf{n}}^{\rm inc}$. Then the polarized signal recorded by detector 2 per unit time is given by

$$\textbf{Signal 2} = \Delta S \mathbf{I}^{\rm sca}(r\hat{\mathbf{n}}^{\rm sca}), \tag{23}$$

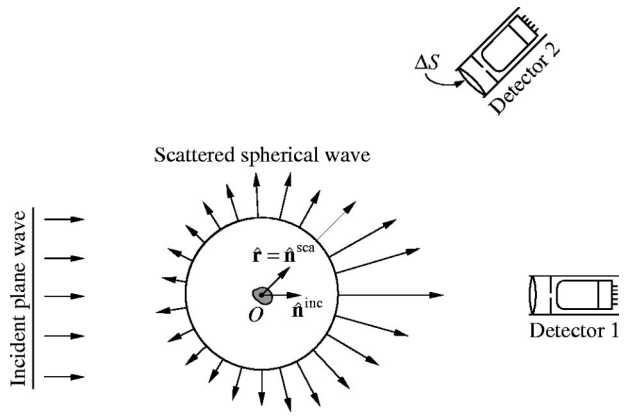

Fig. 4. The response of a collimated detector depends on the line of sight.

where ΔS is the acceptance area of the detector, and the Stokes vector of the scattered light is expressed in that of the incident light by means of the 4×4 phase matrix $\mathbf{Z}$:

$$\mathbf{I}^{\rm sca}(r\hat{\mathbf{n}}^{\rm sca}) = \frac{1}{r^2}\mathbf{Z}(\hat{\mathbf{n}}^{\rm sca}, \hat{\mathbf{n}}^{\rm inc})\mathbf{I}^{\rm inc}. \tag{24}$$

It can be shown that the elements of $\mathbf{Z}(\hat{\mathbf{n}}^{\rm sca}, \hat{\mathbf{n}}^{\rm inc})$ are the following quadratic combinations of the elements of the amplitude matrix $\mathbf{S}(\hat{\mathbf{n}}^{\rm sca}, \hat{\mathbf{n}}^{\rm inc})$:

$$Z_{11} = \tfrac{1}{2}(|S_{11}|^2 + |S_{12}|^2 + |S_{21}|^2 + |S_{22}|^2), \tag{25}$$

$$Z_{12} = \tfrac{1}{2}(|S_{11}|^2 - |S_{12}|^2 + |S_{21}|^2 - |S_{22}|^2), \tag{26}$$

$$Z_{13} = -\mathrm{Re}(S_{11}S_{12}^* + S_{22}S_{21}^*), \tag{27}$$

$$Z_{14} = -\mathrm{Im}(S_{11}S_{12}^* - S_{22}S_{21}^*), \tag{28}$$

$$Z_{21} = \tfrac{1}{2}(|S_{11}|^2 + |S_{12}|^2 - |S_{21}|^2 - |S_{22}|^2), \tag{29}$$

$$Z_{22} = \tfrac{1}{2}(|S_{11}|^2 - |S_{12}|^2 - |S_{21}|^2 + |S_{22}|^2), \tag{30}$$

$$Z_{23} = -\mathrm{Re}(S_{11}S_{12}^* - S_{22}S_{21}^*), \tag{31}$$

$$Z_{24} = -\mathrm{Im}(S_{11}S_{12}^* + S_{22}S_{21}^*), \tag{32}$$

$$Z_{31} = -\mathrm{Re}(S_{11}S_{21}^* + S_{22}S_{12}^*), \tag{33}$$

$$Z_{32} = -\mathrm{Re}(S_{11}S_{21}^* - S_{22}S_{12}^*), \tag{34}$$

$$Z_{33} = \mathrm{Re}(S_{11}S_{22}^* + S_{12}S_{21}^*), \tag{35}$$

$$Z_{34} = \mathrm{Im}(S_{11}S_{22}^* + S_{21}S_{12}^*), \tag{36}$$

$$Z_{41} = -\mathrm{Im}(S_{21}S_{11}^* + S_{22}S_{12}^*), \tag{37}$$

$$Z_{42} = -\mathrm{Im}(S_{21}S_{11}^* - S_{22}S_{12}^*), \tag{38}$$

$$Z_{43} = \mathrm{Im}(S_{22}S_{11}^* - S_{12}S_{21}^*), \tag{39}$$

$$Z_{44} = \mathrm{Re}(S_{22}S_{11}^* - S_{12}S_{21}^*). \tag{40}$$

All elements of the phase matrix are real valued and have the dimension of area.

To describe the response of detector 1, we need to introduce the Stokes parameters of the total field for propagation directions $\hat{\mathbf{r}}$ very close to $\hat{\mathbf{n}}^{\rm sca}$:

$$\mathbf{I}(r\hat{\mathbf{r}}) = \frac{1}{2}\left(\frac{\varepsilon_1}{\mu_0}\right)^{1/2}\begin{pmatrix} E_\theta(r\hat{\mathbf{r}})[E_\theta(r\hat{\mathbf{r}})]^* + E_\varphi(r\hat{\mathbf{r}})[E_\varphi(r\hat{\mathbf{r}})]^* \\ E_\theta(r\hat{\mathbf{r}})[E_\theta(r\hat{\mathbf{r}})]^* - E_\varphi(r\hat{\mathbf{r}})[E_\varphi(r\hat{\mathbf{r}})]^* \\ -E_\theta(r\hat{\mathbf{r}})[E_\varphi(r\hat{\mathbf{r}})]^* - E_\varphi(r\hat{\mathbf{r}})[E_\theta(r\hat{\mathbf{r}})]^* \\ \mathrm{i}\{E_\varphi(r\hat{\mathbf{r}})[E_\theta(r\hat{\mathbf{r}})]^* - E_\theta(r\hat{\mathbf{r}})[E_\varphi(r\hat{\mathbf{r}})]^*\} \end{pmatrix}, \tag{41}$$

where the total electric field is given by $\mathbf{E}(r\hat{\mathbf{r}}) = \mathbf{E}^{\mathrm{inc}}(r\hat{\mathbf{r}}) + \mathbf{E}^{\mathrm{sca}}(r\hat{\mathbf{r}})$. Then the polarized signal recorded by detector 1 per unit time is obtained by integrating $\mathbf{I}(r\hat{\mathbf{r}})$ over the sensitive surface of the detector:

$$\textbf{Signal 1} = \int_{\Delta S} \mathrm{d}S\, \mathbf{I}(r\hat{\mathbf{r}}) = \Delta S \mathbf{I}^{\mathrm{inc}} - \mathbf{K}(\hat{\mathbf{n}}^{\mathrm{inc}})\mathbf{I}^{\mathrm{inc}} + \Delta S \frac{1}{r^2}\mathbf{Z}(\hat{\mathbf{n}}^{\mathrm{inc}}, \hat{\mathbf{n}}^{\mathrm{inc}})\mathbf{I}^{\mathrm{inc}}, \tag{42}$$

where the elements of the forward-scattering phase matrix $\mathbf{Z}(\hat{\mathbf{n}}^{\mathrm{inc}}, \hat{\mathbf{n}}^{\mathrm{inc}})$ and the 4×4 extinction matrix $\mathbf{K}(\hat{\mathbf{n}}^{\mathrm{inc}})$ are expressed in those of the forward-scattering amplitude matrix $\mathbf{S}(\hat{\mathbf{n}}^{\mathrm{inc}}, \hat{\mathbf{n}}^{\mathrm{inc}})$ according to Eqs. (25)–(40) and the formulas

$$K_{jj} = \frac{2\pi}{k_1}\mathrm{Im}(S_{11} + S_{22}), \qquad j = 1,\ldots,4, \tag{43}$$

$$K_{12} = K_{21} = \frac{2\pi}{k_1}\mathrm{Im}(S_{11} - S_{22}), \tag{44}$$

$$K_{13} = K_{31} = -\frac{2\pi}{k_1}\mathrm{Im}(S_{12} + S_{21}), \tag{45}$$

$$K_{14} = K_{41} = \frac{2\pi}{k_1}\mathrm{Re}(S_{21} - S_{12}), \tag{46}$$

$$K_{23} = -K_{32} = \frac{2\pi}{k_1}\mathrm{Im}(S_{21} - S_{12}), \tag{47}$$

$$K_{24} = -K_{42} = -\frac{2\pi}{k_1}\mathrm{Re}(S_{12} + S_{21}), \tag{48}$$

$$K_{34} = -K_{43} = \frac{2\pi}{k_1}\mathrm{Re}(S_{22} - S_{11}). \tag{49}$$

The elements of the Stokes extinction matrix are real valued and have the dimension of area.

By placing detector 1 sufficiently far from the scatterer, one can make negligible the contribution of the third term on the right-hand side of Eq. (42):

$$\textbf{Signal 1} \underset{r\to\infty}{=} \Delta S \mathbf{I}^{\mathrm{inc}} - \mathbf{K}(\hat{\mathbf{n}}^{\mathrm{inc}})\mathbf{I}^{\mathrm{inc}}. \tag{50}$$

As a consequence, the extinction matrix becomes a directly observable quantity.

It is important to note that the scattering pattern for particles comparable with and larger than the wavelength is known to change dramatically when the scattering direction varies by as little as $\pi/(2k_1a)$ (rad) (see, e.g., pp. 234–236 of Ref. 1 and Fig. 7.3 and plates 9.1 and 10.1 of MTL). Therefore, if a detector were to fully resolve this angular variability, the distance r from the particle to the detector would have to satisfy the inequality

$$\frac{\pi}{2k_1a} \gg \frac{D}{2r}, \tag{51}$$

where D is the diameter of the acceptance area of the detector. This practical requirement supplements the theoretical far-field zone criteria (9)–(11). If this requirement is not met, then the detector will record a convolution of the angular scattering pattern with the detector angular aperture.

E. Optical Cross Sections

Important derivative characteristics of the particle are the total optical cross sections, which are defined as follows. The product of the scattering cross section C_{sca} and the incident monochromatic energy flux gives the total monochromatic power removed from the incident wave owing to scattering of the incident radiation by the particle in all directions. The product of the absorption cross section C_{abs} and the incident monochromatic energy flux is equal to the total monochromatic power removed from the incident wave as a result of absorption of light by the particle. Finally, the product of the extinction cross section C_{ext} and the incident monochromatic energy flux gives the total monochromatic power removed by the particle from the incident light on account of the combined effect of scattering and absorption.

Explicit formulas for the extinction and scattering cross sections follow from Eqs. (22), (24), and (50):

$$C_{\mathrm{sca}} = \frac{1}{I^{\mathrm{inc}}}\int_S \mathrm{d}S\, I^{\mathrm{sca}}(\mathbf{r}) = \frac{1}{I^{\mathrm{inc}}}\int_{4\pi} \mathrm{d}\hat{\mathbf{r}}[Z_{11}(\hat{\mathbf{r}}, \hat{\mathbf{n}}^{\mathrm{inc}})I^{\mathrm{inc}} + Z_{12}(\hat{\mathbf{r}}, \hat{\mathbf{n}}^{\mathrm{inc}})Q^{\mathrm{inc}} + Z_{13}(\hat{\mathbf{r}}, \hat{\mathbf{n}}^{\mathrm{inc}})U^{\mathrm{inc}} + Z_{14}(\hat{\mathbf{r}}, \hat{\mathbf{n}}^{\mathrm{inc}})V^{\mathrm{inc}}], \tag{52}$$

$$C_{\mathrm{ext}} = \frac{1}{I^{\mathrm{inc}}}[K_{11}(\hat{\mathbf{n}}^{\mathrm{inc}})I^{\mathrm{inc}} + K_{12}(\hat{\mathbf{n}}^{\mathrm{inc}})Q^{\mathrm{inc}} + K_{13}(\hat{\mathbf{n}}^{\mathrm{inc}})U^{\mathrm{inc}} + K_{14}(\hat{\mathbf{n}}^{\mathrm{inc}})V^{\mathrm{inc}}], \tag{53}$$

where S is the surface of a sphere centered at the scattering particle and having a radius r large enough to be in the particle far-field zone and $\mathrm{d}\hat{\mathbf{r}} = \mathrm{d}S/r^2$ is an infinitesimal solid angle element around the direction $\hat{\mathbf{r}}$. The absorption cross section is equal to the difference of the extinction and scattering cross sections:

$$C_{\mathrm{abs}} = C_{\mathrm{ext}} - C_{\mathrm{sca}} \geqslant 0. \tag{54}$$

3. SINGLE-SCATTERING APPROXIMATION FOR A FIXED GROUP OF PARTICLES

We will now consider electromagnetic scattering by an arbitrary fixed group of N finite particles (Fig. 5). In this case, one can express the total electric field $\mathbf{E}(\mathbf{r})$ everywhere in space in terms of the vector version of the Foldy–Lax equations[19]:

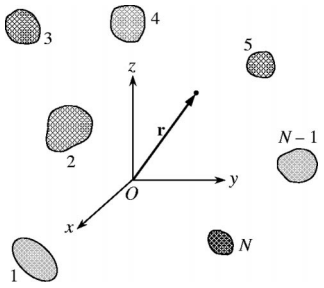

Fig. 5. Scattering by a fixed configuration of N finite particles.

$$\mathbf{E}(\mathbf{r}) = \mathbf{E}^{\mathrm{inc}}(\mathbf{r}) + \sum_{i=1}^{N} \int_{V_i} d\mathbf{r}' \, \vec{G}(\mathbf{r}, \mathbf{r}') \cdot \int_{V_i} d\mathbf{r}'' \, \vec{T}_i(\mathbf{r}', \mathbf{r}'') \cdot \mathbf{E}_i(\mathbf{r}''), \qquad \mathbf{r} \in \Re^3, \tag{55}$$

where $\mathbf{r}$ is the position vector originating at the origin of the common (laboratory) coordinate system, V_i is the volume occupied by particle i, the electric field $\mathbf{E}_i(\mathbf{r})$ that is "exciting" particle i is given by

$$\mathbf{E}_i(\mathbf{r}) = \mathbf{E}^{\mathrm{inc}}(\mathbf{r}) + \sum_{j(\neq i)=1}^{N} \mathbf{E}_{ij}^{\mathrm{exc}}(\mathbf{r}), \tag{56}$$

the $\mathbf{E}_{ij}^{\mathrm{exc}}(\mathbf{r})$ are partial exciting fields given by

$$\mathbf{E}_{ij}^{\mathrm{exc}}(\mathbf{r}) = \int_{V_j} d\mathbf{r}' \, \vec{G}(\mathbf{r}, \mathbf{r}') \cdot \int_{V_j} d\mathbf{r}'' \, \vec{T}_j(\mathbf{r}', \mathbf{r}'') \cdot \mathbf{E}_j(\mathbf{r}''), \qquad \mathbf{r} \in V_i, \tag{57}$$

and $\vec{T}_i$ is the ith-particle dyad transition operator with respect to the laboratory coordinate system. The Foldy–Lax equations (55)–(57) directly follow from the Maxwell equations and provide an exact description of multiple scattering by the N-particle group. Indeed, Eq. (55) expresses the total field everywhere in space in terms of the vector sum of the incident field and the partial fields generated by each particle in response to the corresponding exciting fields, whereas Eqs. (56) and (57) show that the field exciting each particle consists of the incident field and the fields generated by all other particles. Importantly, each $\vec{T}_i$ satisfies Eq. (8) and is, therefore, the dyad transition operator of particle i in the absence of all other particles.

Let us now assume that the second term on the right-hand side of Eq. (56) is small in comparison with the first term. This means that each particle is excited only by the external incident field, which is the definition of the single-scattering approximation (SSA) for the fixed N-particle aggregate. We then have, instead of Eq. (55),

$$\mathbf{E}(\mathbf{r}) = \mathbf{E}^{\mathrm{inc}}(\mathbf{r}) + \mathbf{E}^{\mathrm{sca}}(\mathbf{r}), \qquad \mathbf{r} \in \Re^3, \tag{58}$$

where the total scattered field is a vector sum of the partial scattered fields:

$$\mathbf{E}^{\mathrm{sca}}(\mathbf{r}) = \sum_{i=1}^{N} \mathbf{E}_i^{\mathrm{sca}}(\mathbf{r}), \tag{59}$$

$$\mathbf{E}_i^{\mathrm{sca}}(\mathbf{r}) = \int_{V_i} d\mathbf{r}' \, \vec{G}(\mathbf{r}, \mathbf{r}') \cdot \int_{V_i} d\mathbf{r}'' \, \vec{T}_i(\mathbf{r}', \mathbf{r}'') \cdot \mathbf{E}^{\mathrm{inc}}(\mathbf{r}''). \tag{60}$$

It is clear that each partial field is independent of the partial fields scattered by all other particles forming the group [cf. Eq. (7)].

Let us choose the origin O of the laboratory coordinate system close to the geometrical center of the group, illuminate the fixed N-particle group by a plane electromagnetic wave incident in the direction of the unit vector $\hat{\mathbf{s}}$, i.e.,

$$\mathbf{E}^{\mathrm{inc}}(\mathbf{r}) = \mathbf{E}_0^{\mathrm{inc}} \exp(ik_1 \hat{\mathbf{s}} \cdot \mathbf{r}), \qquad \mathbf{E}_0^{\mathrm{inc}} \cdot \hat{\mathbf{s}} = 0, \tag{61}$$

assume that the observation point is located in the far-field zone of any particle forming the group (Fig. 6), and recall Eqs. (14) and (15). The latter indicate that the outgoing spherical wave generated by particle i in response to a plane-wave excitation of the form $\mathbf{E}_0^{\mathrm{inc}} \exp(ik_1 \hat{\mathbf{s}} \cdot \mathbf{r}_i)$ in the far-field zone of this particle is given by $r_i^{-1} \exp(ik_1 r_i) \vec{A}_i(\hat{\mathbf{r}}_i, \hat{\mathbf{s}}) \cdot \mathbf{E}_0^{\mathrm{inc}}$, where $\mathbf{r}_i$ originates inside particle i (Fig. 6), $\vec{A}_i(\hat{\mathbf{r}}_i, \hat{\mathbf{s}})$ is the ith-particle scattering dyad centered at the particle origin, and $\hat{\mathbf{r}}_i = \mathbf{r}_i / r_i$ is the unit vector in the scattering direction. To make use of this fact, we must rewrite Eq. (61) in the form

$$\mathbf{E}^{\mathrm{inc}}(\mathbf{r}) = \mathbf{E}_0^{\mathrm{inc}} \exp(ik_1 \hat{\mathbf{s}} \cdot \mathbf{r}_i) \exp(ik_1 \hat{\mathbf{s}} \cdot \mathbf{R}_i), \tag{62}$$

where $\mathbf{R}_i$ connects the origin of the laboratory coordinate system with the origin of particle i (Fig. 6). This gives

$$\mathbf{E}_i^{\mathrm{sca}}(\mathbf{r}) = \exp(ik_1 \hat{\mathbf{s}} \cdot \mathbf{R}_i) \frac{\exp(ik_1 r_i)}{r_i} \vec{A}_i(\hat{\mathbf{r}}_i, \hat{\mathbf{s}}) \cdot \mathbf{E}_0^{\mathrm{inc}}. \tag{63}$$

This formula is valid provided that the inequalities (9)–(11) hold for each particle of the group.

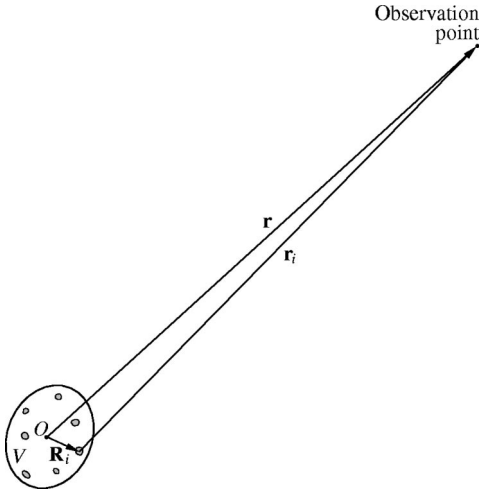

Fig. 6. Far-field scattering by a collection of particles.

4. FAR-FIELD SINGLE-SCATTERING APPROXIMATION FOR A FIXED PARTICLE GROUP

Assuming that $r \gg R_i$ for any i yields

$$r_i = |\mathbf{r} - \mathbf{R}_i| = r\left(1 - \frac{2\hat{\mathbf{r}}\cdot\mathbf{R}_i}{r} + \frac{R_i^2}{r^2}\right)^{1/2} \approx r - \hat{\mathbf{r}}\cdot\mathbf{R}_i + \frac{R_i^2}{2r}. \quad (64)$$

Therefore

$$\mathbf{E}_i^{\mathrm{sca}}(\mathbf{r}) = \frac{\exp(ik_1 r)}{r}\exp(i\Delta_i)\vec{A}_i(\hat{\mathbf{r}},\hat{\mathbf{s}})\cdot\mathbf{E}_0^{\mathrm{inc}}, \quad (65)$$

where

$$\Delta_i = k_1(\hat{\mathbf{s}} - \hat{\mathbf{r}})\cdot\mathbf{R}_i, \quad (66)$$

and it is further assumed that $r \gg k_1 R_i^2/2$ and $\vec{A}_i(\hat{\mathbf{r}}_i,\hat{\mathbf{s}}) \approx \vec{A}_i(\hat{\mathbf{r}},\hat{\mathbf{s}})$. We can now rewrite Eq. (59) as

$$\mathbf{E}^{\mathrm{sca}}(\mathbf{r}) = \frac{\exp(ik_1 r)}{r}\vec{A}(\hat{\mathbf{r}},\hat{\mathbf{s}})\cdot\mathbf{E}_0^{\mathrm{inc}}, \quad (67)$$

where the scattering dyad of the entire volume element is given by

$$\vec{A}(\hat{\mathbf{r}},\hat{\mathbf{s}}) = \sum_{i=1}^{N}\exp(i\Delta_i)\vec{A}_i(\hat{\mathbf{r}},\hat{\mathbf{s}}). \quad (68)$$

It is clear that Eq. (67) describes a transverse outgoing spherical wave centered at O. Exploiting the transverse character of the wave yields

$$\mathbf{E}^{\mathrm{sca}}(\mathbf{r}) = \frac{\exp(ik_1 r)}{r}\mathbf{S}(\hat{\mathbf{r}},\hat{\mathbf{s}})\cdot\mathbf{E}_0^{\mathrm{inc}}, \quad (69)$$

where we have used the notation of Eq. (19), and the total amplitude matrix of the group $\mathbf{S}(\hat{\mathbf{r}},\hat{\mathbf{s}})$ is expressed in terms of the partial amplitude matrices $\mathbf{S}_i(\hat{\mathbf{r}},\hat{\mathbf{s}})$ centered at the respective particle origins as

$$\mathbf{S}(\hat{\mathbf{r}},\hat{\mathbf{s}}) = \sum_{i=1}^{N}\exp(i\Delta_i)\mathbf{S}_i(\hat{\mathbf{r}},\hat{\mathbf{s}}). \quad (70)$$

The approximate equality $\vec{A}_i(\hat{\mathbf{r}}_i,\hat{\mathbf{s}}) \approx \vec{A}_i(\hat{\mathbf{r}},\hat{\mathbf{s}})$ used to derive Eq. (67) means that the angular pattern of light scattering by each single particle is assumed to change insignificantly over the range of scattering directions equal to the angular size of the volume element V collectively occupied by the particles (Fig. 6) as viewed from the observation point. Therefore the distance r from the volume element to the observation point must satisfy the inequality $\pi/(2k_1 a_i) \gg L_{\max}/2r$, where $L_{\max}$ is the maximal linear dimension of the volume element [cf. the inequality (51)]. On the other hand, the assumption $r \gg R_i$ leads to the inequality $r \gg L_{\max}/2$.

In what follows, we will assume for simplicity that the volume element V is roughly equidimensional so that its minimal ($L_{\min}$) and maximal ($L_{\max}$) linear dimensions are approximately the same: $L_{\min} \approx L_{\max} \approx L$, where L is a "typical" linear dimension of the volume element. It is then clear from our derivation and discussion that the criteria of applicability of Eqs. (69) and (70) can be summarized as follows:

$$r \gg \max\left(\frac{L}{2}, \frac{Lk_1 a_i}{\pi}\right) \quad \text{or} \quad r \gg \max\left(\frac{L}{2}, \frac{2La_i}{\lambda_1}\right), \quad i = 1,\ldots,N, \quad (71)$$

$$r \gg \frac{k_1 L^2}{8}, \quad (72)$$

$$k_1 r \gg 1, \quad (73)$$

where $\lambda_1 = 2\pi/k_1$ is the wavelength in the surrounding medium. The inequalities (72) and (73) are quite similar to the last two criteria of far-field scattering by a single particle, the inequalities (10) and (11), the only difference being that the radius a of the smallest circumscribing sphere of the particle in the inequalities (10) and (11) is now replaced by $L/2$. As before, the inequality (72) requires the observation point to be so far from the volume element that the phase difference between the paths connecting the observation point and any two particles of the group becomes independent of r. As a consequence, the surfaces of constant phase of the partial waves generated by the individual particles coincide, and the waves form a single outgoing spherical wave. Thus Eqs. (69) and (70) are valid only if the observation point is located in the far-field zone of the entire N-particle configuration.

Equations (69) and (70) are the main result of the far-field SSA for a fixed N-particle group. They show that in the far-field zone of the entire group, the total scattered electric field becomes a single outgoing spherical wave, and the scattering process can be described by a single amplitude matrix centered at the common origin of the group. This allows one to introduce the extinction and phase matrices and the optical cross sections of the group as a whole in complete analogy with how it was done in Section 2 for a single particle and to model the electromagnetic response of a detector located in the far-field zone of the entire group.

In particular, since the Δ_i vanish in the exact forward-scattering direction ($\hat{\mathbf{r}} = \hat{\mathbf{s}}$), substituting Eq. (70) into Eqs. (43)–(49) and (53) yields

$$\mathbf{K} = \sum_{i=1}^{N}\mathbf{K}_i, \quad (74)$$

$$C_{\mathrm{ext}} = \sum_{i=1}^{N}(C_{\mathrm{ext}})_i. \quad (75)$$

In other words, the extinction matrix and the extinction cross section of the fixed N-particle group in the framework of the far-field SSA are obtained by adding the respective optical characteristics of all the individual particles forming the group. One can also substitute Eq. (70) into Eqs. (25)–(40) and derive the corresponding formulas for the elements of the total phase matrix. However, we will not do that explicitly but rather will derive a formula for the total phase matrix under additional simplifying assumptions.

5. FAR-FIELD UNCORRELATED SINGLE-SCATTERING APPROXIMATION AND MODIFIED UNCORRELATED SINGLE-SCATTERING APPROXIMATION

Let us now make two further assumptions:

1. The N particles filling the volume element V move during the time necessary to take a measurement in such a way that their positions are random and uncorrelated with each other.
2. The criteria of validity of Eqs. (69) and (70) are satisfied at each moment during the measurement.

Collectively, these assumptions define what can be called the far-field uncorrelated single-scattering approximation (USSA) for a small volume element. Obviously, these assumptions do not change Eqs. (74) and (75), since the latter are independent of the specific particle positions at any moment during the measurement. Therefore Eqs. (74) and (75) are also the formulas for the time-averaged total extinction matrix and extinction cross section of the volume element.

Our next step is to substitute Eq. (70) into Eqs. (25)–(40) and assume that the randomness of particle positions during the measurement leads to the following inequalities:

$$\left\langle \left| \mathrm{Re} \sum_{i=1}^{N} \sum_{i'(\neq i)=1}^{N} [\mathbf{S}_i(\hat{\mathbf{r}}, \hat{\mathbf{s}})]_{kl} [\mathbf{S}_{i'}(\hat{\mathbf{r}}, \hat{\mathbf{s}})]^*_{pq} \exp[\mathrm{i}(\Delta_i - \Delta_{i'})] \right| \right\rangle \ll \left| \mathrm{Re} \sum_{i=1}^{N} [\mathbf{S}_i(\hat{\mathbf{r}}, \hat{\mathbf{s}})]_{kl} [\mathbf{S}_i(\hat{\mathbf{r}}, \hat{\mathbf{s}})]^*_{pq} \right|, \quad (76)$$

and, if $k \neq p$ or $l \neq q$,

$$\left\langle \left| \mathrm{Im} \sum_{i=1}^{N} \sum_{i'(\neq i)=1}^{N} [\mathbf{S}_i(\hat{\mathbf{r}}, \hat{\mathbf{s}})]_{kl} [\mathbf{S}_{i'}(\hat{\mathbf{r}}, \hat{\mathbf{s}})]^*_{pq} \exp[\mathrm{i}(\Delta_i - \Delta_{i'})] \right| \right\rangle \ll \left| \mathrm{Im} \sum_{i=1}^{N} [\mathbf{S}_i(\hat{\mathbf{r}}, \hat{\mathbf{s}})]_{kl} [\mathbf{S}_i(\hat{\mathbf{r}}, \hat{\mathbf{s}})]^*_{pq} \right|, \quad k, l, p, q = 1, 2, \quad (77)$$

where the angle brackets denote the configurational average (an average over the varying particle positions) or, equivalently, the average over a sufficiently long period of time. Equation (66) suggests that for the left-hand sides of the inequalities (76) and (77) to vanish, the positions of particles i and i' must change randomly by approximately a wavelength or more, thereby causing the real and imaginary parts of $\exp(\Delta_i - \Delta_{i'})$ to vary randomly between -1 and 1. It is then straightforward to show that the configurational (or time) average of the total phase matrix of the volume element is also given by the "incoherent" sum of the partial phase matrices:

$$\mathbf{Z} = \sum_{i=1}^{N} \mathbf{Z}_i . \quad (78)$$

Finally, Eqs. (52), (54), and (75) yield the configuration-averaged (or time-averaged) total scattering and absorption cross sections of the volume element as sums of the respective partial optical characteristics:

$$C_{\mathrm{sca}} = \sum_{i=1}^{N} (C_{\mathrm{sca}})_i , \quad (79)$$

$$C_{\mathrm{abs}} = \sum_{i=1}^{N} (C_{\mathrm{abs}})_i . \quad (80)$$

Although the presence of the rapidly oscillating exponential factors indeed causes the left-hand sides of the inequalities (76) and (77) to vanish upon configurational averaging in most cases, it is clear that both inequalities are violated in the vicinity of the exact forward-scattering direction ($\hat{\mathbf{r}} \approx \hat{\mathbf{s}}$), when all the Δ_i vanish or become very small [cf. Eq. (66)] and all the exponential factors $\exp[\mathrm{i}(\Delta_i - \Delta_{i'})]$ reduce to unity. This means that single scattering by constituent particles in directions close to the exact forward direction is always coherent or almost coherent irrespective of specific particle positions and must result in an additional enhancement of intensity due to constructive interference.[24,25] Therefore Eqs. (78)–(80) are *not* a direct consequence of the USSA but rather are based on the USSA and the additional assumption that the forward-scattering interference can be neglected. The latter assumption, along with the USSA, defines the far-field modified uncorrelated single-scattering approximation (MUSSA) for a small volume element.

Equations (74), (75), and (78)–(80) are usually adopted without rigorous proof and form the basis for treating single scattering by random particle ensembles in virtually every book on light scattering and radiative transfer. It is clear from our detailed derivation that Eqs. (74) and (75) are a consequence of the simple far-field SSA as applied to any particle group, either fixed or random, whereas Eqs. (78)–(80) are strictly valid only in the framework of the far-field MUSSA.

Spatial coordinates are not the only particle characteristics that can vary with time. If the particles are nonspherical, they can also change their orientation with respect to the laboratory coordinate system. Depending on their chemical composition, the particles can also change their shapes and sizes owing to oscillations of liquid-droplet surfaces or owing to the processes of evaporation, condensation, sublimation, and melting. Even the total number of particles in the volume element can change during the time necessary to take the measurement. A traditional approach in such cases is to assume that temporal changes of particle states (represented collectively by their sizes, shapes, orientations, and refractive indices) are totally uncorrelated with temporal changes of their coordinates. As a consequence, one may average the right-hand sides of Eqs. (74), (75), and (78)–(80) over the varying particle states and obtain the following formulas for the cumulative ensemble-averaged optical characteristics of the entire volume element:

$$\mathbf{K} = N\langle \mathbf{K} \rangle, \quad (81)$$

$$\mathbf{Z} = N\langle \mathbf{Z} \rangle, \quad (82)$$

$$C_{\mathrm{ext}} = N\langle C_{\mathrm{ext}} \rangle, \quad (83)$$

$$C_{\rm sca} = N\langle C_{\rm sca}\rangle, \tag{84}$$

$$C_{\rm abs} = N\langle C_{\rm abs}\rangle, \tag{85}$$

where N is the average number of particles in the volume element during the time of the measurement and the angle brackets denote averages of the respective single-particle characteristics over the particle states.

Finally, we remark that although the formulas of Sections 3–5 have been derived assuming that the incident field is a plane electromagnetic wave, the reader can easily verify that all results remain the same if the incident radiation is a parallel quasi-monochromatic beam of light.

6. FORWARD-SCATTERING INTERFERENCE

To demonstrate the forward-scattering interference effect, Fig. 7 shows the element F_{11} of the scattering matrix for a simple two-sphere system in random orientation computed with the exact superposition T-matrix method.[26] Following MTL, the scattering matrix is defined as

$$\mathbf{F}(\Theta) = \mathbf{Z}(\theta^{\rm sca} = \Theta,\ \varphi^{\rm sca} = 0;\ \ \theta^{\rm inc} = 0,\ \varphi^{\rm inc} = 0). \tag{86}$$

Averaging over the uniform orientation distribution of the two-sphere cluster is intended to approximately model the randomness of the component sphere positions relative to each other. Also shown are the results for two equivalent spheres that scatter light in total isolation from each other.

It is clearly seen indeed that the main difference between the curves for two interacting spheres and those for two noninteracting spheres is the presence of a pronounced oscillating pattern at forward-scattering angles. To demonstrate unequivocally that the latter is caused by the interference, we note that, as follows from Eqs. (25)–(40), (66), and (70), the interference contributions ($i \neq i'$) to the total phase matrix of a two-sphere cluster differ from the incoherent contributions ($i = i'$) in that each of them includes an additional factor $\exp[ik_1(\hat{\mathbf{s}} - \hat{\mathbf{r}}) \cdot (\mathbf{R}_1 - \mathbf{R}_2)]$ or $\exp[-ik_1(\hat{\mathbf{s}} - \hat{\mathbf{r}}) \cdot (\mathbf{R}_1 - \mathbf{R}_2)]$, where $\mathbf{R}_1$ and $\mathbf{R}_2$ connect the origin of the laboratory coordinate system with the centers of spheres 1 and 2, respectively. By writing $\mathbf{R}_2 - \mathbf{R}_1 = \mathbf{d} = d\hat{\mathbf{d}}$, where d is the distance between the component sphere centers and the unit vector $\hat{\mathbf{d}}$ specifies the cluster orientation, and averaging over all $\hat{\mathbf{d}}$, we derive

$$\begin{aligned}\frac{1}{4\pi}\int_{4\pi} d\hat{\mathbf{d}} \exp[-ik_1 d(\hat{\mathbf{s}} - \hat{\mathbf{r}}) \cdot \hat{\mathbf{d}}] &= \frac{1}{4\pi}\int_{4\pi} d\hat{\mathbf{d}} \exp[ik_1 d(\hat{\mathbf{s}} - \hat{\mathbf{r}}) \cdot \hat{\mathbf{d}}] \\ &= \frac{\sin(k_1 d|\hat{\mathbf{s}} - \hat{\mathbf{r}}|)}{k_1 d|\hat{\mathbf{s}} - \hat{\mathbf{r}}|} \\ &= f(\Theta),\end{aligned} \tag{87}$$

where $\Theta = \arccos(\hat{\mathbf{r}} \cdot \hat{\mathbf{s}})$ is the scattering angle and

$$f(\Theta) = \frac{\sin[2k_1 d \sin(\Theta/2)]}{2k_1 d \sin(\Theta/2)}, \tag{88}$$

since $|\hat{\mathbf{s}} - \hat{\mathbf{r}}| = 2\sin(\Theta/2)$ as shown in Fig. 8. Thus the total two-sphere phase and scattering matrices in the SSA are given by

$$\mathbf{Z}(\hat{\mathbf{r}},\ \hat{\mathbf{s}}) = 2\mathbf{Z}_1(\hat{\mathbf{r}},\ \hat{\mathbf{s}})[1 + f(\Theta)], \tag{89}$$

$$\mathbf{F}(\Theta) = 2\mathbf{F}_1(\Theta)[1 + f(\Theta)], \tag{90}$$

where $\mathbf{Z}_1(\hat{\mathbf{r}},\ \hat{\mathbf{s}})$ and $\mathbf{F}_1(\Theta)$ are the single-sphere phase and scattering matrices, respectively. Figure 9 demonstrates that for a sufficiently large value of $k_1 d$, these simple formulas provide a nearly perfect fit to the exact T-matrix result. $f(\Theta)$ has a sharp and narrow maximum at $\Theta = 0$ followed by a succession of maxima and minima with decreasing frequency and magnitude (see Fig. 10). The magnitude of all maxima and minima is inversely proportional to $k_1 d$, with the exception of the first interference maximum at $\Theta = 0$, whose magnitude is always equal to unity owing to the well-known limit $(\sin x)/x \underset{x\to 0}{\to} 1$.

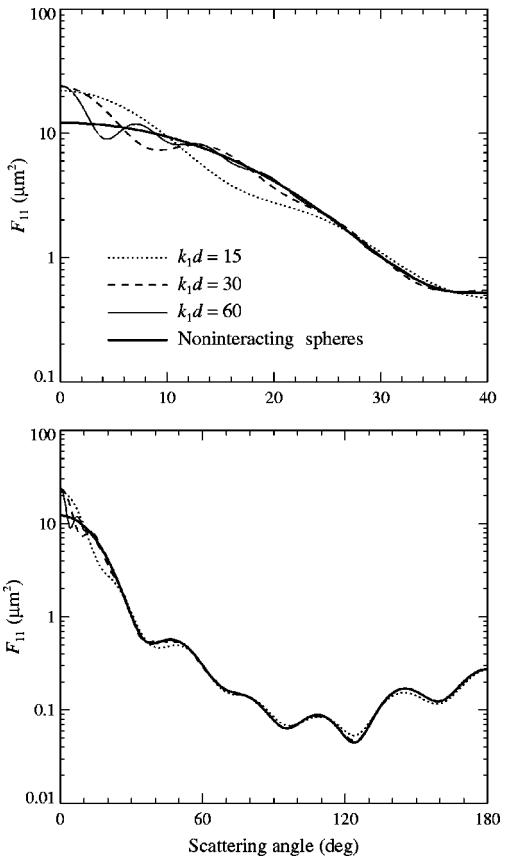

Fig. 7. Results of exact T-matrix computations of the F_{11} element of the scattering matrix versus scattering angle Θ for a two-sphere cluster in random orientation. The distance d between the centers of the component spheres increases such that the product $k_1 d$ grows from 15 to 60. The radius of each sphere is $a = 0.5\ \mu$m, their relative refractive index is $m = 1.5$, and the wavelength in the surrounding medium is $\lambda_1 = 2\pi/k_1 = 0.6283\ \mu$m. For comparison, the thick curves show the F_{11} element for two noninteracting spheres of the same size and relative refractive index.

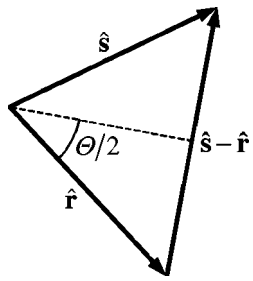

Fig. 8. Illustration of the equality $|\hat{\mathbf{s}} - \hat{\mathbf{r}}| = 2\sin(\Theta/2)$.

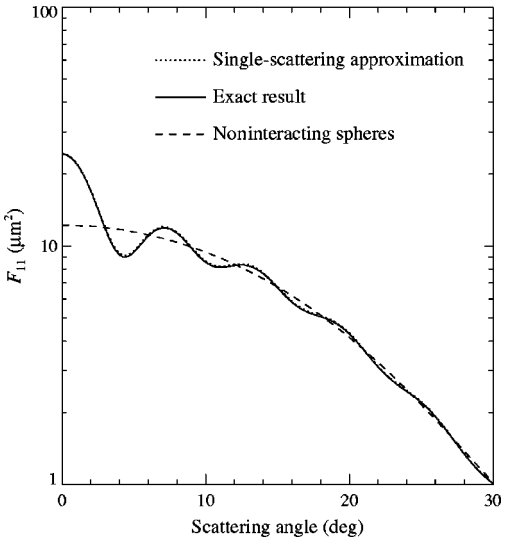

Fig. 9. The solid curve shows the results of exact T-matrix computations of the F_{11} element of the scattering matrix versus the scattering angle Θ for a two-sphere cluster in random orientation with $k_1 d = 60$, $a = 0.5\ \mu$m, $m = 1.5$, and $\lambda_1 = 0.6283\ \mu$m. For comparison, the dotted curve shows the result of using Eq. (90), whereas the dashed curve depicts the F_{11} element for two noninteracting spheres of the same size and relative refractive index.

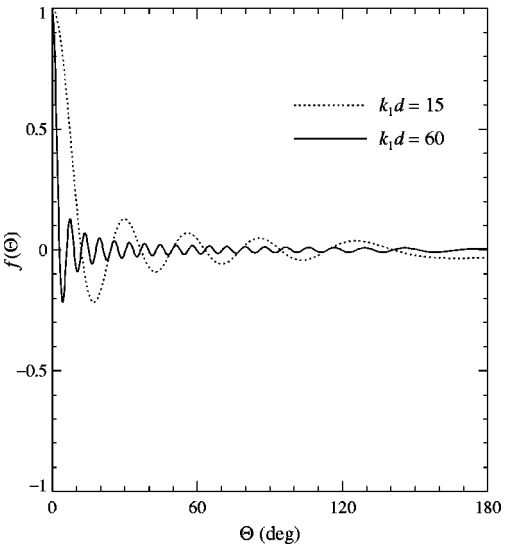

Fig. 10. $f(\Theta)$ versus Θ for $k_1 d = 15$ and 60.

This explains the diminishing effect of the interference with increasing $k_1 d$ and Θ at side-scattering and backscattering angles in Fig. 7.

If the distance between the sphere centers changes during the measurement, then one must average $f(\Theta)$ over a range $d \in [d_{\min}, d_{\max}]$. This can be done easily, provided that all d values are equiprobable, by using the well-known formula $\int dx\, x^{-1} \sin x = \mathrm{si}(x)$, where $\mathrm{si}(x)$ is the sine integral.[27]

7. ENERGY CONSERVATION

As we have mentioned above, the presence of the interference pattern at forward-scattering angles means that Eqs. (78)–(80) for the configuration-averaged total phase matrix and total scattering and absorption cross sections are only approximate consequences of the far-field USSA. Unfortunately, this also implies that the USSA violates the energy conservation law. Indeed, energy conservation requires that the total scattering cross section of the particle collection, C_{sca}, be equal to the total extinction cross section C_{ext} if all the constituent particles are nonabsorbing, so that $(C_{\mathrm{sca}})_i = (C_{\mathrm{ext}})_i$ for each i. One can see that Eqs. (75) and (79) already lead to $C_{\mathrm{sca}} = C_{\mathrm{ext}}$, even though Eq. (79) does not include the contribution of the forward-scattering interference pattern. Adding this contribution brakes the energy balance and leads to the unphysical result $C_{\mathrm{sca}} \neq C_{\mathrm{ext}}$.

The fact that the MUSSA satisfies the energy conservation law precisely whereas the presumably more accurate USSA does not seems to be rather strange. The explanation of this paradox is that the USSA includes two-particle electromagnetic interactions in the calculation of the total phase matrix and the total scattering cross section but not in the calculation of the total extinction matrix and the total extinction cross section. It can in fact be shown that energy conservation is restored if one takes into account two-particle interactions in the calculation of $\mathbf{K}$ and C_{ext} by including the contribution of light scattered twice, but this goes beyond the framework of the SSA. Therefore the implicit way to ensure energy conservation in the MUSSA is to artificially ignore the forward-scattering interference.

8. CONDITIONS OF VALIDITY OF THE FAR-FIELD MODIFIED UNCORRELATED SINGLE-SCATTERING APPROXIMATION

Let us now consider what happens with increasing average distance $\langle d \rangle$ between neighboring particles in a random group. Figure 7 shows that increasing the distance between two interacting spheres makes the main interference maximum narrower, whereas the F_{11} values at other scattering angles approach those obtained by doubling the corresponding single-sphere F_{11} values. Also, it is seen that the $F_{11}(0)$ value for two interacting spheres remains approximately constant with varying distance between the sphere centers and is close to twice that computed for two noninteracting spheres, as it should be [the square of the sum of two equal electric fields is equal to twice the sum of the squares of the fields: $|\mathbf{E} + \mathbf{E}|^2 = 2(|\mathbf{E}|^2 + |\mathbf{E}|^2)$]. Thus we can conclude that the expected consequences of taking the limit $k_1 \langle d \rangle \to \infty$ are the following:

- The total amount of energy contained in the interference pattern decreases with increasing interparticle distance and eventually becomes negligible compared with the total energy scattered by the particles.
- The angular width of the main interference peak becomes so small that the peak becomes hardly distinguishable from the incident beam.

As a consequence, the MUSSA gives essentially the same results as those from the USSA as far as most practical applications of light scattering are concerned.

The first zero of the function $f(\Theta)$ occurs at $\Theta = \Theta_0 = 2\arcsin[\pi/(2k_1d)]$. Therefore, to make the amount of energy contained in the interference pattern for a two-particle system negligibly small, this angle must be much smaller than π, which means that k_1d must be much greater than unity. Furthermore, it is well-known that at least half of the energy scattered by large particles ($k_1a \gg 1$) is contained in the narrow diffraction peak and mostly at scattering angles $\Theta < 4/(k_1a)$ (see Sec. 7.4 of MTL). Therefore we must also require that $\Theta_0 \ll 4/(k_1a)$, which leads to $d \gg a$.

Although the forward-scattering interference pattern for a many-particle system can be significantly more complex than that shown in Figs. 7 and 9, it is clear that the conditions of validity of Eqs. (78)–(80) imposed by the presence of the pattern should be as follows:

$$\langle d\rangle \gg \langle a\rangle, \tag{91}$$

$$k_1L \gg 1, \tag{92}$$

where $\langle d\rangle$ is the average distance between neighboring particles and $\langle a\rangle$ is the average particle size. The inequality (92) reflects the obvious fact that the angular width of the forward-scattering interference peak generated by a many-particle group is controlled by the average distance between any two particles from the group rather than that between two neighboring particles. Note that the inequality (91) is also needed to ensure that particle positions are uncorrelated during the measurement (the position of each particle is not affected by the presence of the other particles).

Let us now discuss the conditions of validity of the main assumption of the SSA, viz., that each particle is excited only by the incident field. Obviously, when particles are located close to each other, the field scattered by one particle can modify the total field exciting another particle. For example, if the line connecting the centers of two particles is nearly parallel to the incidence direction, then the field scattered by the particle located closer to the source of illumination can attenuate the incident field when it reaches the other particle. For particles much larger than the wavelength, this effect can be qualitatively interpreted as a "shadow" cast by the first particle upon the second particle.

To illustrate this phenomenon, Fig. 11 shows the results of T-matrix computations of the ratio ρ of the total scattering cross section for a two-particle cluster with identical touching components and in random orientation to the sum of the scattering cross sections of two noninteracting spheres as a function of the sphere size parameter k_1a. In the geometrical-optics limit, the scattering cross section of a nonabsorbing particle is equal to twice the area of the particle projection onto the plane perpendicular to the incidence direction (see Sec. 7.4 of MTL). Therefore, in the limit $k_1a \to \infty$, the ratio ρ should approach the value $\langle G\rangle/(2\pi a^2)$, where $\langle G\rangle$ is the orientation average of the projected area of the two-sphere cluster. Obviously, ρ would be very close to unity if the distance between the sphere centers were much greater than their radii, but it should be significantly smaller than unity for touching spheres.

Figure 12 illustrates the computation of $\langle G\rangle$ for the case of a randomly oriented two-sphere cluster with identical touching components. As before, the cluster orientation is specified by the direction of the unit vector $\hat{\mathbf{d}}$ or, equivalently, by its polar angle θ and azimuth angle φ [Fig. 12(a)]. Let us assume for the sake of simplicity that the incident light propagates in the direction of the positive z axis. Then the area of the bisphere projection onto the xy plane is independent of the azimuth angle, so that

$$\begin{aligned}\langle G\rangle &= \frac{1}{4\pi}\int_{4\pi} d\hat{\mathbf{d}}\, G(\hat{\mathbf{d}})\\ &= \frac{1}{4\pi}\int_0^{2\pi} d\varphi \int_0^{\pi} d\theta\, \sin\theta\, G(\theta)\\ &= \int_0^{\pi/2} d\theta\, \sin\theta\, G(\theta),\end{aligned} \tag{93}$$

where $G(\theta)$ is the area of the shape shown in Fig. 12(b). Obviously, the latter is equal to $2\pi a^2$ minus twice the common area of the two overlapping circles in Fig. 12(c), or $G(\theta) = a^2(\pi/2 - \theta - \sin\theta\cos\theta)$, thereby yielding $\langle G\rangle/(2\pi a^2) = 1/2 + 4/(3\pi) \approx 0.9244$. The actual scattering cross-section ratio in Fig. 11 indeed tends to this asymptotic value as the size parameter increases, thereby corroborating the presence and the importance of the shadowing effect.

The requirement that the contribution of the scattered light to the field exciting each particle be negligible rela-

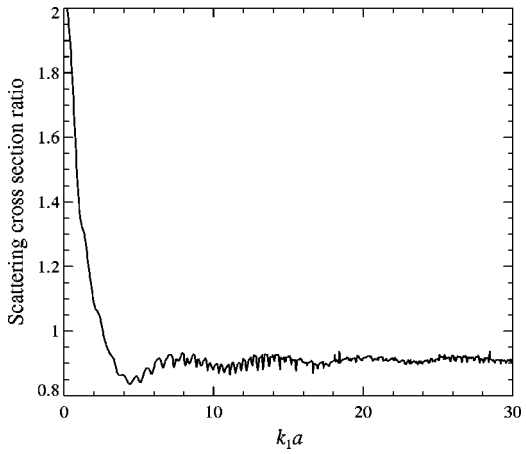

Fig. 11. Ratio of the total scattering cross section for a two-particle cluster with identical touching components and in random orientation to the sum of the scattering cross sections of two noninteracting spheres of the same radius as a function of the sphere size parameter. The relative refractive index of the spheres is 1.5.

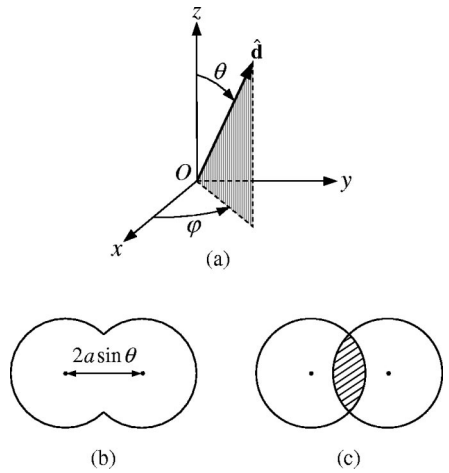

Fig. 12. Computation of $\langle G \rangle$ for a randomly oriented cluster consisting of two identical touching spheres.

tive to the external incident field also limits the total number of particles in the group. Obviously, the total amount of energy scattered by the particles filling a volume element must be much smaller than the amount of incident energy passing through the volume-element cross section:

$$\sum_{i=1}^{N} (C_{\mathrm{sca}})_i \ll L^2. \tag{94}$$

The forward-scattering interference and the shadowing effect are not the only manifestations of the electromagnetic interaction between the particles forming a group and not the only factors that limit the accuracy of the far-field MUSSA and its range of applicability in terms of the smallest allowable interparticle separation. Unfortunately, it is difficult to perform a more detailed theoretical analysis of this problem for many-particle clusters composed of arbitrary particles. We hope, therefore, that exact numerical results for a few simple cases can provide at least qualitative guidance (see also Refs. 28 and 29).

Figure 13 depicts the ratio of the total scattering cross section of a two-sphere cluster in random orientation to that of two noninteracting spheres of the same size. It is clear that in order for this ratio to be sufficiently close to unity, the distance between the centers of the interacting spheres must be at least several times greater than the sphere radii. The corresponding asymmetry parameter ratio (Fig. 14) is much closer to unity and is essentially independent of $k_1 d$ for the larger spheres with $x = 5$ and 10 but still requires interparticle distances $d \gg a$ for the spheres with $x = 1$ in order to reach the asymptotic value unity.

Figures 7 and 15 demonstrate how increasing the interparticle separation affects the scattering matrix element F_{11} and the ratios F_{22}/F_{11} and $-F_{21}/F_{11}$ for two interacting wavelength-sized spheres. The behavior of the ratio F_{22}/F_{11} is especially revealing, since it must be identically equal to unity for noninteracting spheres. Obviously, this asymptotic regime is approximately reached when the distance between the sphere centers exceeds several times their radii. We have seen above that no distance between the interacting spheres can eliminate the forward-scattering interference pattern (Fig. 7). However, this pattern becomes very narrow when d exceeds several times the sphere radii (or several times the wavelength for subwavelength-sized particles) and eventually becomes indistinguishable from the incident light. Although the data depicted in Figs. 7 and 13–15 were computed for two-sphere clusters with equal components, analogous T-matrix results for bispheres with different components (not shown here) exhibit the same basic features and lead to the same conclusions.

Our final note concerns the relative importance of the far-field-zone criteria (10) and (72) for a single particle and for a particle collection, respectively. For a single particle with a size parameter $k_1 a = 10$, the inequality (10) implies that the far-field zone begins at a distance from the particle much greater than five particle radii, which is not much stricter than the inequality (9). However, for a volume element with a size parameter $k_1 L/2 = 10^4$, the inequality (72) yields $r \gg 0.25 \times 10^4 L$, which

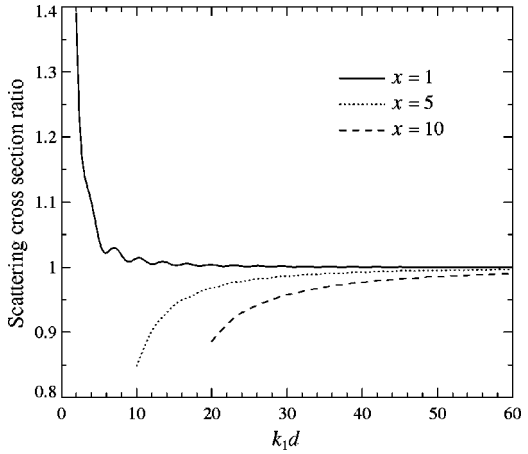

Fig. 13. Ratio of the scattering cross section of a two-sphere cluster with equal components and in random orientation to the sum of the scattering cross sections of two noninteracting spheres of the same radius as a function of $k_1 d$. The relative refractive index of the spheres is 1.5, and their size parameter $x = k_1 a$ varies from 1 to 10.

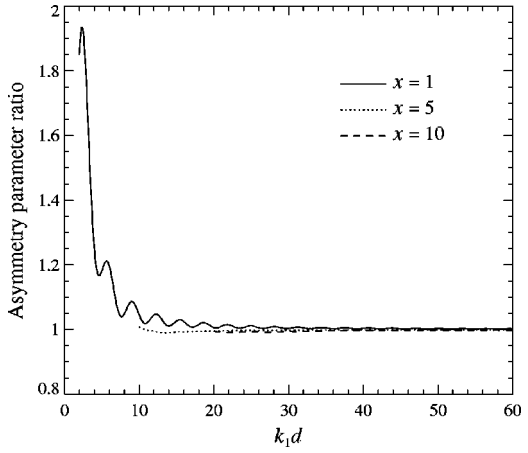

Fig. 14. Same as Fig. 13, but for the ratio of the asymmetry parameter of a two-sphere cluster with equal components and in random orientation to the asymmetry parameter of two noninteracting spheres of the same radius.

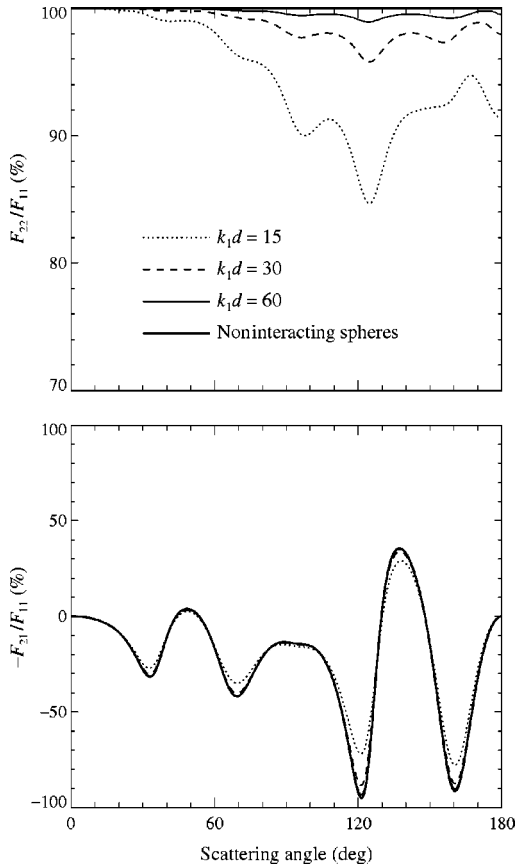

Fig. 15. Same as Fig. 7, but for the ratios F_{22}/F_{11} and $-F_{21}/F_{11}$.

moves the far-field zone much farther from the volume element than the inequalities (71) and (73) would require. This implies that if one wants to apply the MUSSA to a volume element with $L = 2$ mm, assuming a source of illumination with a wavelength of 0.6283 μm (thereby yielding $k_1 L/2 = 10^4$), then the observation point must be moved from the volume element by many meters. However, Section 9 will demonstrate that in many circumstances, one can theoretically model the response of a detector located at a distance much greater than the volume-element size but not as far as the inequality (72) would necessitate.

9. FIRST-ORDER-SCATTERING APPROXIMATION

In this section, we will take another look at single scattering of light by a small volume element by assuming that detectors of the scattered light are located sufficiently far from the volume element that the inequalities (9)–(11) are satisfied for each particle and the inequalities (71) and (73) are also valid, whereas the inequality (72) will not be enforced. As a consequence, the volume element can no longer be considered a single scatterer and characterized by total extinction and phase matrices.

As before, we start with the SSA equations (58), (59), and (63). We then define the coherency dyad of the total electric field at the observation point as

$$\begin{aligned}\vec{\rho}(\mathbf{r}) &= \mathbf{E}(\mathbf{r}) \otimes \mathbf{E}^*(\mathbf{r}) \\ &= \mathbf{E}^{\rm inc}(\mathbf{r}) \otimes [\mathbf{E}^{\rm inc}(\mathbf{r})]^* + \mathbf{E}^{\rm inc}(\mathbf{r}) \otimes \sum_{i=1}^{N} [\mathbf{E}_i^{\rm sca}(\mathbf{r})]^* \\ &\quad + \sum_{i=1}^{N} [\mathbf{E}_i^{\rm sca}(\mathbf{r})] \otimes [\mathbf{E}^{\rm inc}(\mathbf{r})]^* + \sum_{i=1}^{N} [\mathbf{E}_i^{\rm sca}(\mathbf{r})] \\ &\quad \otimes \sum_{j(\neq i)=1}^{N} [\mathbf{E}_j^{\rm sca}(\mathbf{r})]^* + \sum_{i=1}^{N} [\mathbf{E}_i^{\rm sca}(\mathbf{r})] \otimes [\mathbf{E}_i^{\rm sca}(\mathbf{r})]^* \end{aligned} \tag{95}$$

and assume that during the time necessary to take a measurement, the positions of all particles inside the volume V are totally random, so that the probability to find particle i within the elementary volume $d\mathbf{R}_i$ centered at $\mathbf{R}_i$ is equal to $p_{\mathbf{R}}(\mathbf{R}_i)d\mathbf{R}_i$, where

$$p_{\mathbf{R}}(\mathbf{R}_i) = \begin{cases} 1/V & \text{if } \mathbf{R}_i \in V \\ 0 & \text{if } \mathbf{R}_i \notin V \end{cases}. \tag{96}$$

The total randomness of particle positions implies that the average distance between neighboring particles is much greater than the particle sizes:

$$\langle d \rangle \gg a_i, \qquad i = 1,...,N. \tag{97}$$

Thus the configuration-averaged coherency dyad is given by

$$\begin{aligned}\langle \vec{\rho}(\mathbf{r}) \rangle &= \mathbf{E}^{\rm inc}(\mathbf{r}) \otimes [\mathbf{E}^{\rm inc}(\mathbf{r})]^* + \mathbf{E}^{\rm inc}(\mathbf{r}) \otimes \sum_{i=1}^{N} \langle [\mathbf{E}_i^{\rm sca}(\mathbf{r})]^* \rangle \\ &\quad + \sum_{i=1}^{N} \langle [\mathbf{E}_i^{\rm sca}(\mathbf{r})] \rangle \otimes [\mathbf{E}^{\rm inc}(\mathbf{r})]^* + \sum_{i=1}^{N} \langle [\mathbf{E}_i^{\rm sca}(\mathbf{r})] \rangle \\ &\quad \otimes \sum_{j(\neq i)=1}^{N} \langle [\mathbf{E}_j^{\rm sca}(\mathbf{r})]^* \rangle + \sum_{i=1}^{N} \langle [\mathbf{E}_i^{\rm sca}(\mathbf{r})] \\ &\quad \otimes [\mathbf{E}_i^{\rm sca}(\mathbf{r})]^* \rangle. \end{aligned} \tag{98}$$

The first term on the right-hand side of this formula is the coherency dyad of the incident field, the second and third terms describe the interference of the incident and scattered fields, the fourth term describes the interference of the partial fields singly scattered by different particles, and the fifth term is the sum of the coherency dyads of the partial scattered fields.

Averaging the interference terms over particle positions involves the evaluation of the integrals

$$\begin{aligned}\langle \mathbf{E}_i^{\rm sca}(\mathbf{r}) \rangle &= \int_{\Re^3} d\mathbf{R}_i \, p_{\mathbf{R}}(\mathbf{R}_i) \mathbf{E}_i^{\rm sca}(\mathbf{r}) \\ &= \int_{\Re^3} d\mathbf{R}_i \, p_{\mathbf{R}}(\mathbf{R}_i) \exp(ik_1 \hat{\mathbf{s}} \cdot \mathbf{R}_i) \\ &\quad \times \frac{\exp(ik_1 r_i)}{r_i} \vec{A}_i(\hat{\mathbf{r}}_i, \hat{\mathbf{s}}) \cdot \mathbf{E}_0^{\rm inc} \end{aligned} \tag{99}$$

[cf. Eq. (63)], which give the average partial scattered fields at the observation point. It is convenient to perform the integration in the spherical coordinate system

originating at the observation point [Fig. 16(a)]. Taking into account that $\mathbf{R}_i = \mathbf{r} + \mathbf{R}_i'$, where the vector $\mathbf{R}_i'$ connects the observation point and particle i, and using the Saxon asymptotic expression,[30] given by

$$\exp(ik_1\hat{\mathbf{s}}\cdot\mathbf{R}_i') \underset{k_1R_i'\to\infty}{=} \frac{i2\pi}{k_1R_i'}[\delta(\hat{\mathbf{s}}+\hat{\mathbf{R}}_i')\exp(-ik_1R_i') - \delta(\hat{\mathbf{s}}-\hat{\mathbf{R}}_i')\exp(ik_1R_i')], \quad (100)$$

we obtain

$$\langle\mathbf{E}_i^{\mathrm{sca}}(\mathbf{r})\rangle = \frac{i2\pi}{k_1}\int_{4\pi}d\hat{\mathbf{R}}_i'\int_0^\infty dR_i'[\delta(\hat{\mathbf{s}}+\hat{\mathbf{R}}_i') - \delta(\hat{\mathbf{s}}-\hat{\mathbf{R}}_i')\exp(2ik_1R_i')]p_{\mathbf{R}}(\mathbf{R}_i) \times \vec{A}_i(-\hat{\mathbf{R}}_i',\hat{\mathbf{s}})\cdot\mathbf{E}^{\mathrm{inc}}(\mathbf{r}). \quad (101)$$

This formula shows that each average partial scattered field is contributed to only by those points of the volume element that belong to the segment $\Delta s(\mathbf{r})$ of the infinite line through the observation point and the source of illumination [Figs. 16(a) and 16(b)]. Hence the following three situations must be considered: The observation point can either be behind the scattering volume as viewed from the source of illumination [e.g., point 1 in Fig. 16(b)], be between the source of illumination and the scattering volume (e.g., point 2), or lie on a line that is parallel to the incidence direction and does not go through the scattering volume (e.g., point 3).

It is obvious that $\langle\mathbf{E}_i^{\mathrm{sca}}(\mathbf{r}_3)\rangle$ is equal to zero and that

$$\langle\mathbf{E}_i^{\mathrm{sca}}(\mathbf{r}_1)\rangle = \frac{i2\pi}{k_1V}\Delta s(\mathbf{r}_1)\vec{A}_i(\hat{\mathbf{s}},\hat{\mathbf{s}})\cdot\mathbf{E}^{\mathrm{inc}}(\mathbf{r}_1). \quad (102)$$

The radial integral for point 2 contains a rapidly oscillating factor $\exp(2ik_1R_i')$, which makes $\langle\mathbf{E}_i^{\mathrm{sca}}(\mathbf{r}_2)\rangle$ much smaller than $\langle\mathbf{E}_i^{\mathrm{sca}}(\mathbf{r}_1)\rangle$ provided that $k_1\Delta s(\mathbf{r}_2)\gg 1$. The latter condition is equivalent to the inequality (92). Thus $\langle\mathbf{E}_i^{\mathrm{sca}}(\mathbf{r})\rangle$ is given by Eq. (102) if the observation point is "shadowed" by the volume element and vanishes otherwise.

It is clear from Eqs. (16) and (102) that the average partial field created by particle i at a shadowed distant observation point is a transverse plane wave propagating in the direction of the incident plane wave. Therefore the second and third terms on the right-hand side of Eq. (98) describe the interference of pairs of transverse plane waves propagating in the same direction.

It follows from Eqs. (20), (43)–(46), and (53) that the factor $(2\pi/k_1V)\Delta s(\mathbf{r}_1)\Sigma_{i=1}^N\vec{A}_i(\hat{\mathbf{s}},\hat{\mathbf{s}})$ is of the same order of magnitude as that of the sum of the extinction cross sections of all the particles filling the volume element divided by the volume element's geometrical cross section: $\Sigma_{i=1}^N(C_{\mathrm{ext}})_i/L^2$. Assuming that this ratio is much smaller than unity, i.e.,

$$\sum_{i=1}^N(C_{\mathrm{ext}})_i \ll L^2, \quad (103)$$

we can neglect the fourth term on the right-hand side of Eq. (98) in comparison with the second and third terms.

Integrating the last term on the right-hand side of Eq. (98) over all particle positions and recalling the inequality (71) yield $\Sigma_{i=1}^N[\vec{A}_i(\hat{\mathbf{r}},\hat{\mathbf{s}})\cdot\mathbf{E}_0^{\mathrm{inc}}]\otimes[\vec{A}_i(\hat{\mathbf{r}},\hat{\mathbf{s}})\cdot\mathbf{E}_0^{\mathrm{inc}}]^*/r^2$. This is simply an "incoherent" sum of partial coherency dyads at the observation point, each partial dyad being due to a transverse spherical wave propagating in the same direction given by the unit vector $\hat{\mathbf{r}}$.

We can now make use of the transverse character of the plane and spherical waves involved in the first, second, third, and fifth terms on the right-hand side of Eq. (98) and rewrite the latter in terms of the Stokes vector by using Eq. (4). After tedious but simple manipulations, we derive

$$\mathbf{I}(\mathbf{r}) = \mathbf{I}^{\mathrm{inc}} - \frac{\Delta s(\mathbf{r})}{V}\sum_{i=1}^N\mathbf{K}_i(\hat{\mathbf{s}})\mathbf{I}^{\mathrm{inc}} + \frac{1}{r^2}\sum_{i=1}^N\mathbf{Z}_i(\hat{\mathbf{s}},\hat{\mathbf{s}})\mathbf{I}^{\mathrm{inc}} \quad (104a)$$

if the observation point is shadowed by the volume element and

$$\mathbf{I}(\mathbf{r}) = \frac{1}{r^2}\sum_{i=1}^N\mathbf{Z}_i(\hat{\mathbf{r}},\hat{\mathbf{s}})\mathbf{I}^{\mathrm{inc}} \quad (104b)$$

otherwise. We will refer to the totality of approximations made in the derivation of Eqs. (104) as the first-order-scattering approximation (FOSA).

Let us now consider the measurement situation shown schematically in Fig. 16(c), where the diameter D of the

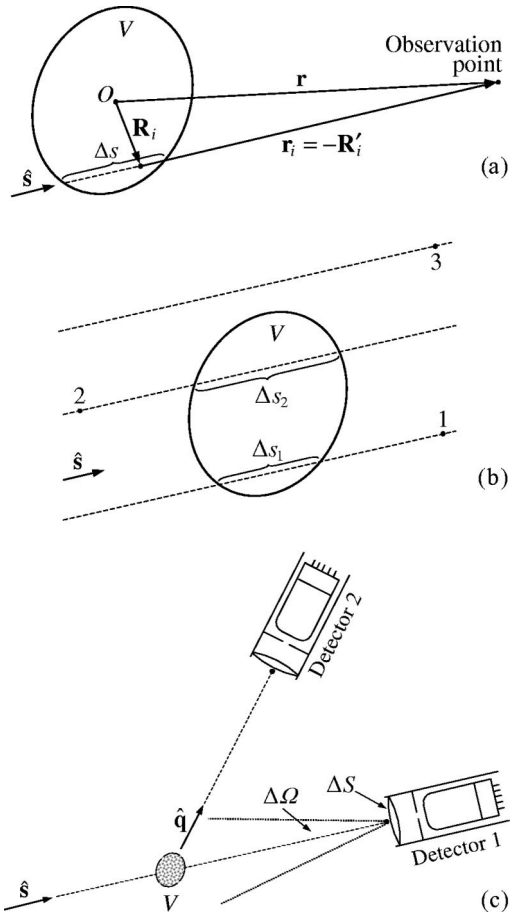

Fig. 16. First-order scattering by a small volume element.

acceptance area of either detector is assumed to be greater than the linear dimension L of the scattering volume and the angular aperture $\Delta\Omega$ of either detector is large enough to encompass the entire scattering volume. Both detectors are located far enough from the volume element to satisfy the inequalities (51) (for each particle), (71), and (73). We can now integrate Eqs. (104) over the acceptance area of the detectors to derive that the polarized signal measured by detector 1 per unit time is given by

$$\textbf{Signal 1} = \Delta S \mathbf{I}^{\mathrm{inc}} - \sum_{i=1}^{N} \mathbf{K}_i(\hat{\mathbf{s}})\mathbf{I}^{\mathrm{inc}} + \frac{\Delta S}{r^2}\sum_{i=1}^{N} \mathbf{Z}_i(\hat{\mathbf{s}}, \hat{\mathbf{s}})\mathbf{I}^{\mathrm{inc}}, \tag{105}$$

whereas that measured by detector 2 per unit time is given by

$$\textbf{Signal 2} = \frac{\Delta S}{r^2}\sum_{i=1}^{N} \mathbf{Z}_i(\hat{\mathbf{q}}, \hat{\mathbf{s}})\mathbf{I}^{\mathrm{inc}}. \tag{106}$$

By choosing r sufficiently large, one can minimize the third term on the right-hand side of Eq. (105) relative to the second term. As a consequence, the response of detector 1 becomes

$$\textbf{Signal 1} = \Delta S \mathbf{I}^{\mathrm{inc}} - \sum_{i=1}^{N} \mathbf{K}_i(\hat{\mathbf{s}})\mathbf{I}^{\mathrm{inc}}. \tag{107}$$

Equations (106) and (107) represent the main result of the FOSA. Comparison with Eqs. (23), (24), (50), (74), and (78) shows that the FOSA predicts essentially the same electromagnetic response of the distant detectors as that given by the far-field MUSSA but without requiring that the detectors be placed as far from the volume element as to satisfy the inequality (72). Like the MUSSA, the FOSA is based on ignoring the interference of light singly scattered by different particles in the forward direction [i.e., the fourth term on the right-hand side of Eq. (98)] and, as a consequence, satisfies the energy conservation law.

Assuming, as before, that the temporal changes of the particle states are uncorrelated with temporal changes of their coordinates, we obtain

$$\textbf{Signal 1} = \Delta S \mathbf{I}^{\mathrm{inc}} - N\langle \mathbf{K}(\hat{\mathbf{s}})\rangle \mathbf{I}^{\mathrm{inc}}, \tag{108}$$

$$\textbf{Signal 2} = \frac{1}{r^2}\Delta S N\langle \mathbf{Z}(\hat{\mathbf{q}}, \hat{\mathbf{s}})\rangle \mathbf{I}^{\mathrm{inc}}, \tag{109}$$

where the angle brackets denote averages of the extinction and phase matrices over the particle states. Again, this is the same result as that predicted by the far-field MUSSA [cf. Eqs. (81) and (82)].

Equations (108) and (109) can also be derived from the (vector) radiative transfer equation [(V)RTE] by assuming that the number of particles is sufficiently small that $|n_0 L\langle \mathbf{K}(\hat{\mathbf{q}})\rangle_{pq}| \ll 1$ and $|n_0 L\langle \mathbf{Z}(\hat{\mathbf{q}}, \hat{\mathbf{q}}')\rangle_{pq}| \ll 1$ for $p, q = 1,\ldots,4$ and for any $\hat{\mathbf{q}}$ and $\hat{\mathbf{q}}'$, where $n_0 = N/V$ is the particle number density (see Ref. 31 for details). This is not surprising, since the derivation of the FOSA in this section is based on the same basic principles of statistical electromagnetics as those for the microphysical derivation of the VRTE in Ref. 19.

A major difference between the RTE as applied to optically thick media and the FOSA is that for the RTE to be valid, the scattering particles must be (1) randomly positioned and uncorrelated and (2) separated far enough apart that each of them is in the far-field zones of all other particles. Such particles were called independently scattering in Ref. 19. This means, in particular, that the average distance between neighboring particles must satisfy inequality (91) as well as inequalities

$$\langle d\rangle \gg \frac{k_1\langle a\rangle^2}{2}, \tag{110}$$

$$k_1\langle d\rangle \gg 1 \tag{111}$$

[cf. inequalities (10) and (11)]. It is easily seen that inequality (110) can become very restrictive for particles with large size parameters. Fortunately, as our derivation demonstrates, condition (110) does not apply to either the MUSSA or the FOSA.

10. DISCUSSION

The traditional way to define the Stokes parameters applies only to transverse electromagnetic waves such as plane and spherical waves. It was, therefore, logical to start the analysis of single scattering by a small volume element using the far-field SSA, which treats the volume element as a united scatterer generating a single outgoing spherical wave and makes possible the introduction of the cumulative amplitude, phase, and extinction matrices.

An important result of our analysis of the far-field SSA applied to a random group of particles is that one must distinguish between the simple USSA and the MUSSA. The MUSSA satisfies the energy conservation law, is widely used in practice, and is a cornerstone of the phenomenological theory of radiative transfer. However, one should be aware of the fact that the MUSSA goes beyond the USSA by neglecting the interference of light scattered by various particles in the vicinity of the exact forward direction and thus may be inapplicable in circumstances involving precise computations or measurements at scattering angles approaching zero (e.g., Ref. 32). Otherwise, the MUSSA can be expected to give satisfactory results provided that the following conditions are met:

1. The observation point is located far enough to satisfy the inequalities (71)–(73).
2. Particle positions are random and uncorrelated and change by approximately a wavelength or more during the time interval necessary to take a measurement.
3. The inequalities (91) and (92) are satisfied.
4. The geometrical cross section of the volume element is much greater than its total scattering cross section [the inequality (94)].

Note that for particle positions to be uncorrelated, the average distance between neighboring particles must be much greater than their sizes, which also leads to the inequality (91). Since for large nonabsorbing particles the scattering cross section is approximately equal to twice

the area of the particle geometrical cross section (e.g., Sec. 7.4 of MTL), the inequality (94) can be rewritten in the form

$$L \gg \langle a \rangle \sqrt{2\pi N}. \tag{112}$$

If the distance from the center of the volume element to the observation point does not satisfy the inequality (72), then the total field scattered by the volume element cannot be approximated by a single spherical wave. In this case, it is impossible to define the phase and extinction matrices of the volume element as a whole, and a different approximate way to model the response of a detector measuring electromagnetic scattering by the small volume element is called for. One such technique is to apply the first-order-scattering approximation, which is based on the following assumptions:

(i) The observation point is located far enough to satisfy the inequalities (71) and (73).

(ii) Particle positions within the volume element are completely random during the time interval necessary to take a measurement [Eq. (96)].

(iii) The inequalities (91) and (92) are satisfied.

(iv) The sum of the extinction cross sections of the particles filling the volume element is much smaller than the volume-element geometrical cross section [the inequality (103)]. For particles larger than the wavelength, this assumption is equivalent to the inequality (94).

We have demonstrated that if these conditions are met, then the FOSA leads to essentially the same result as those from the far-field MUSSA in terms of the polarized response of a distant detector.

We have shown that the inequality (91) is a formal criterion of applicability of both the MUSSA and the FOSA, whereas the most stringent criterion of independent scattering, the inequality (110), can be ignored. To illustrate these inequalities as well as the inequality (111), we consider specific cases of scattering media such as clouds and fog. The first example is a cumulus cloud with $\langle a \rangle = 4\ \mu\text{m}$ and $n_0 = 1000\ \text{cm}^{-3}$ (see, e.g., Ref. 33). Ignoring the finite size of the droplets and using a random-number generator to place the drops randomly inside a 1-cm × 1-cm × 1-cm cubical volume element yield[34] $\langle d \rangle \approx 560\ \mu\text{m} = 140\langle a \rangle$ and $k_1\langle d \rangle \approx 5600$, where we have assumed that $k_1 = 10\ \mu\text{m}^{-1}$, thereby corresponding to a 0.6283-μm wavelength in air. Since $k_1\langle a \rangle = 40$, we can conclude that all the inequalities (91), (110), and (111) are satisfied, which means, in particular, that the cloud droplets are independently scattering particles.

As a second example, let us consider what van de Hulst called a "very dense fog" with $\langle a \rangle = 0.5$ mm and $n_0 = 1\ \text{cm}^{-3}$ (see page 5 of Ref. 1). Now $\langle d \rangle \approx 0.56\ \text{cm} \approx 11.3\langle a \rangle$ (Ref. 34), $k_1\langle d \rangle \approx 56000$, and $k_1\langle a \rangle = 5000$. Obviously, the inequalities (91) and (111) are still satisfied, whereas the inequality (110) is grossly violated. Therefore such particles cannot be formally considered independent scatterers. This does not necessarily mean that the RTE cannot yield multiple-scattering results accurate enough for some practical applications, but it is clear that it should be used with great caution.

In summary, our discussion shows that the far-field MUSSA and the FOSA can be viewed as opposite ways to deal with a small volume element by treating it as a single "random" scatterer and as a small cloud of particles, respectively. Indeed, the MUSSA does and the FOSA does not allow one to define unified extinction and phase matrices of an entire particle group. However, the MUSSA requires that the distance from the volume element to the observation point be large enough to satisfy the inequality (72), whereas the FOSA does not impose this stiff limitation. Most importantly, although the MUSSA and the FOSA are based on somewhat different sets of assumptions, they give practically the same result in terms of the polarized response of a sufficiently distant detector.

Either way to address the problem of electromagnetic scattering by a small volume element filled with randomly positioned particles requires the observation point to be located at a distance much greater than the largest linear dimension of the volume element. This makes highly questionable the applicability of the concept of a small volume element in phenomenological derivations of the RTE because all points of a large volume surrounding the small volume element and violating the inequality (71) must be excluded from consideration. Fortunately, as we have already mentioned, the concept of a small volume element is completely unnecessary if the RTE is consistently derived from the Maxwell equations.[19]

ACKNOWLEDGMENTS

We thank Yuri Barabenenkov, Anatoli Borovoi, Michiel Min, Piet Stammes, Cornelis van der Mee, and Gorden Videen for many fruitful discussions on subjects related to this paper, and we thank Nadia Zakharova for help with graphics. This research was supported by the NASA Radiation Sciences Program managed by Donald Anderson.

Corresponding author Michael Mishchenko can be reached by e-mail at crmim@giss.nasa.gov.

REFERENCES

1. H. C. van de Hulst, *Light Scattering by Small Particles* (Wiley, New York, 1957).
2. M. Kerker, *The Scattering of Light and Other Electromagnetic Radiation* (Academic, New York, 1969).
3. L. P. Bayvel and A. R. Jones, *Electromagnetic Scattering and Its Applications* (Applied Science, London, 1981).
4. C. F. Bohren and D. R. Huffman, *Absorption and Scattering of Light by Small Particles* (Wiley, New York, 1983).
5. M. I. Mishchenko, J. W. Hovenier, and L. D. Travis, eds., *Light Scattering by Nonspherical Particles* (Academic, San Diego, Calif., 2000).
6. A. A. Kokhanovsky, *Optics of Light Scattering Media* (Praxis, Chichester, UK, 2001).
7. M. I. Mishchenko, L. D. Travis, and A. A. Lacis, *Scattering, Absorption, and Emission of Light by Small Particles* (Cambridge U. Press, Cambridge, UK, 2002).
8. F. Borghese, P. Denti, and R. Saija, *Scattering from Model Nonspherical Particles* (Springer, Berlin, 2003).
9. J. E. Hansen and L. D. Travis, "Light scattering in planetary atmospheres," Space Sci. Rev. **16**, 527–610 (1974).
10. H. C. van de Hulst, *Multiple Light Scattering* (Academic, New York, 1980).
11. J. W. Hovenier and C. V. M. van der Mee, "Fundamental re-

lationships relevant to the transfer of polarized light in a scattering atmosphere," Astron. Astrophys. **128**, 1–16 (1983).
12. J. Lenoble, ed., *Radiative Transfer in Scattering and Absorbing Atmospheres* (Deepak, Hampton, Va., 1985).
13. A. K. Fung, *Microwave Scattering and Emission Models and Their Applications* (Artech House, Boston, Mass., 1994).
14. A. Ishimaru, *Wave Propagation and Scattering in Random Media* (IEEE, New York, 1997).
15. E. G. Yanovitskij, *Light Scattering in Inhomogeneous Atmospheres* (Springer, Berlin, 1997).
16. G. E. Thomas and K. Stamnes, *Radiative Transfer in the Atmosphere and Ocean* (Cambridge U. Press, Cambridge, UK, 1999).
17. L. Tsang, J. A. Kong, and K.-H. Ding, *Scattering of Electromagnetic Waves: Theories and Applications* (Wiley, New York, 2000).
18. K. N. Liou, *An Introduction to Atmospheric Radiation* (Academic, San Diego, Calif., 2002).
19. M. I. Mishchenko, "Vector radiative transfer equation for arbitrarily shaped and arbitrarily oriented particles: a microphysical derivation from statistical electromagnetics," Appl. Opt. **41**, 7114–7134 (2002).
20. J. W. Hovenier, "Measuring scattering matrices of small particles at optical wavelengths," in *Light Scattering by Nonspherical Particles*, M. I. Mishchenko, J. W. Hovenier, and L. D. Travis, eds. (Academic, San Diego, Calif., 2000), pp. 355–365.
21. H. Volten, O. Muñoz, E. Rol, J. F. de Haan, W. Vassen, J. W. Hovenier, K. Muinonen, and T. Nousiainen, "Scattering matrices of mineral aerosol particles at 441.6 nm and 632.8 nm," J. Geophys. Res. **106**, 17375–17402 (2001).
22. O. Muñoz, H. Volten, J. F. de Haan, W. Vassen, and J. W. Hovenier, "Experimental determination of scattering matrices of randomly oriented fly ash and clay particles at 442 and 633 nm," J. Geophys. Res. **106**, 22833–22844 (2001).
23. J. W. Hovenier, H. Volten, O. Muñoz, W. J. van der Zande, and L. B. F. M. Waters, "Laboratory studies of scattering matrices for randomly oriented particles: potentials, problems, and perspectives," J. Quant. Spectrosc. Radiat. Transf. **79/80**, 741–755 (2003).
24. K. S. Shifrin, *Scattering of Light in a Turbid Medium* (National Aeronautics and Space Administration, Washington, D.C., 1968).
25. P. Ivanov and A. Ya. Khairullina, "On the coherent scattering of light," Opt. Spectrosc. **23**, 83–86 (1967).
26. M. I. Mishchenko and D. W. Mackowski, "Light scattering by randomly oriented bispheres," Opt. Lett. **19**, 1604–1606 (1994).
27. M. Abramowitz and I. A. Stegun, eds., *Handbook of Mathematical Functions* (Dover, New York, 1965).
28. M. I. Mishchenko, D. W. Mackowski, and L. D. Travis, "Scattering of light by bispheres with touching and separated components," Appl. Opt. **34**, 4589–4599 (1995).
29. A. Quirantes, F. Arroyo, and J. Quirantes-Ros, "Multiple light scattering by spherical particle systems and its dependence on concentration: a *T*-matrix study," J. Colloid Interface Sci. **240**, 78–82 (2001).
30. D. S. Saxon, "Lectures on the scattering of light," Sci. Rep. 9 (Department of Meteorology, University of California at Los Angeles, Los Angeles, Calif., 1955).
31. M. I. Mishchenko, "Microphysical approach to polarized radiative transfer: extension to the case of an external observation point," Appl. Opt. **42**, 4963–4967 (2003).
32. A. P. Ivanov, A. Ya. Khairullina, and T. N. Kharkova, "Experimental detection of cooperative effects in a scattering volume," Opt. Spectrosc. **28**, 204–207 (1970).
33. M. Hess, P. Koepke, and I. Schult, "Optical properties of aerosols and clouds: the software package OPAC," Bull. Am. Meteorol. Soc. **79**, 831–844 (1998).
34. M. Min, University of Amsterdam, Amsterdam, The Netherlands (personal communication, 2003).

ERRATUM

Page 78, 5th line before Eq. (78). $\exp(\Delta_i - \Delta_{i'})$ should read $\exp[i(\Delta_i - \Delta_{i'})]$.